







Synaptic enrichment of pSer129 α -synuclein correlates with dopaminergic denervation in early-stage Parkinson's disease

Received: 6 January 2025

Accepted: 11 June 2025

Published online: 18 July 2025

 Check for updates

Irene Frigerio ^{1,2}✉, Martino L. Morella ^{1,2}, Amber B. Winkelaar¹,
Danai T. Vorgia ¹, John JP Brevé¹, Walter A. Boiten^{1,2}, Bram L. van der Gaag^{1,2},
Ismael L. Calandri^{1,3}, Allert J. Jonker¹, Henk W. Berendse^{2,4}, Daniel Mona⁵,
Markus Britschgi ⁵, Laura E. Jonkman ^{1,2} & Wilma DJ van de Berg ^{1,2}

In Parkinson's disease (PD), α -synuclein aggregation in striatal synapses is hypothesised to trigger a cascade of events leading to synaptic loss and cortical Lewy body (LB) pathology. Using multiplex immunofluorescence and confocal microscopy on 69 brains spanning Braak stages 0–6—including controls, incidental LB disease (iLBD), and PD—we show that phosphorylated (pSer129) α -synuclein is enriched in putaminal dopaminergic synapses already in early disease stages, and associates with dopaminergic terminal loss. C-terminally truncated (CTT122) α -synuclein shows a similar trend in later stages. Enrichment of pSer129 and CTT122 α -synuclein in cortical glutamatergic synapses in the putamen occurs prior to LB appearance in cortical regions, supporting the theory of α -synuclein retrograde transport from synapse to cell body. Using AlphaLISA, we confirm that isolated PD putaminal synaptosomes contain higher pSer129 α -synuclein protein levels compared to controls. These findings suggest that synaptic enrichment of pSer129 α -synuclein occurs in early PD, possibly contributing to dopaminergic denervation and cortical LB pathology.

Parkinson's disease (PD) is the second most common neurodegenerative disorder, affecting more than 6 million individuals globally¹. Clinically, PD is diagnosed when the classical motor symptoms bradykinesia, tremor and/or rigidity, appear². PD is also characterised by a wide range of non-motor symptoms³, which can precede the motor symptoms by 10–15 years during the prodromal phase of the disease⁴. A definite diagnosis of PD can only be established post-mortem, when neurons present with Lewy bodies (LBs) and Lewy neurites (LNs),

abnormal intraneuronal features that are enriched with α -synuclein. Severe loss of nigral dopaminergic neurons⁵ and their synaptic terminals⁶ occurs in PD. This loss can reach 50% by the time patients develop motor symptoms and are being diagnosed⁷. Understanding the early pathological changes that precede widespread LB pathology and dopaminergic denervation may aid in the identification of novel diagnostic biomarkers and therapeutic strategies to halt or slow down the disease process. Previous post-mortem studies suggest that α -

¹Department of Anatomy and Neurosciences, Section Clinical Neuroanatomy and Biobanking, Amsterdam UMC, Vrije Universiteit Amsterdam, Amsterdam, Netherlands. ²Amsterdam Neuroscience, Neurodegeneration, Amsterdam, Netherlands. ³Department of Neurology, Alzheimer Center Amsterdam, Amsterdam, Netherlands. ⁴Department of Neurology, Amsterdam UMC, Vrije Universiteit Amsterdam, Amsterdam, Netherlands. ⁵Roche Pharma Research and Early Development; Neuroscience and Rare Diseases Discovery and Translational Area, Roche Innovation Center Basel, Basel, Switzerland.

✉ e-mail: i.frigerio@amsterdamumc.nl

synuclein accumulation and aggregation in the synapse is an early phenomenon in PD, which contributes not only to loss of synapses and connectivity, but also to the progression of the disease⁸. More insight into synaptic degeneration and α -synuclein accumulation in early disease stages is needed.

At the time of death, LB pathology is observed in approximately 8–17% of normal individuals without clinical records of neurological or psychiatric disorders^{9–12}. These cases are defined as incidental LB disease (iLBD), and are hypothesised to represent a pre-motor stage of LB disease^{4,9,11}. Accumulation of pathological α -synuclein at pre-synaptic terminals has been hypothesised to occur already in the earliest stages of PD, and lead to synaptic loss and retrograde axonal and neuronal degeneration⁸. In physiological states, α -synuclein resides primarily in the presynaptic compartment¹³. In several cellular and animal models of PD, certain α -synuclein proteoforms exert toxic effects in synapses^{14,15}. Moreover, in vitro and in vivo models suggest that propagation of α -synuclein pathology is facilitated by neuronal activity¹⁶, and that a pathological form of α -synuclein might propagate trans-synaptically from neuron to neuron¹⁷. Whether α -synuclein enrichment in synaptic terminals precedes LB pathology in anatomically connected regions in the human brain, remains unanswered.

Many post-translational modifications (PTMs) of α -synuclein, which accumulate in the diseased brain, have been described in ref. 18. Phosphorylation at Serine 129 (pSer129) and C-Terminal Truncation (CTT) are among the α -synuclein PTMs which have gained the most interest. These PTMs have been shown to be increased in PD brains compared to non-diseased controls^{18,19}, to be enriched in LBs²⁰, and are discussed to be involved in α -synuclein aggregation^{13,18,21}. pSer129 α -synuclein was detected in synaptic-enriched fractions in PD²² and at pre- and post-synapses of dementia with Lewy body (DLB) cases²³. Similarly, α -synuclein CTT at residue 122 (CTT122) was found to accumulate in synapses of transgenic mice²⁴. It remains unclear which of these α -synuclein proteoforms, if any, accumulate in striatal synaptic terminals in the human brain, and at what stage in the disease this occurs. Understanding which α -synuclein PTMs are enriched at synaptic sites in the initial phase of the disease could be relevant for the development of biomarkers and effective disease-modifying therapeutic strategies targeting α -synuclein.

Here, we investigated whether certain α -synuclein proteoforms are enriched in pre- and post-synaptic terminals in the putamen prior to overt synaptic degeneration and cortical LB pathology in neuropathological stages of PD. Using multiplex immunofluorescence and high-resolution confocal microscopy, we detected α -synuclein (Syn1, residues 91–99) and two of its PTMs (pSer129 and CTT122) in DAT⁺ and VGLUT1⁺ pre-synaptic, and PSD95⁺ post-synaptic terminals in the putamen of 69 brain donors spanning across Braak α -synuclein stages. In addition, we quantified total, pSer129, and CTT122 α -synuclein protein levels in putaminal synaptosome fractions using *in-house* developed AlphaLISA immunoassays in a subset of the same donors. Our results suggest that synaptic enrichment of pSer129 α -synuclein is already increased in early stages of PD and precedes dopaminergic synaptic loss and cortical LB pathology. In late PD stages, enriched pSer129 α -synuclein in putaminal pre-synaptic and post-synaptic terminals is accompanied by CTT122 α -synuclein.

Results

Cohort demographics

Demographic and pathological data of the brain donors are summarised in Table 1 per group, in Table 2 per Braak α -synuclein stage, and in Supplementary Table 1 per donor. Age ($p < 0.001$) and sex ($p = 0.015$) were significantly different between iLBD, PD and control groups. Post-hoc tests revealed that iLBD donors were significantly older than controls (85 ± 8 vs 76 ± 6 years, $p = 0.004$) and PD donors (85 ± 8 vs 77 ± 8 years, $p = 0.001$), and were mostly females compared to the mostly male PD group (F%: 63% vs 26%, $p = 0.038$). Post-mortem

delay ($p = 0.3$), Thal phase (A score; $p = 0.3$) and Braak NFT stage (B score; $p = 0.14$) were similar between groups. PD donors had an average disease duration of 16 years. Sex ($p = 0.4$), post-mortem delay ($p = 0.4$), Thal phase (A score; $p = 0.11$), and Braak NFT stage (B score; $p = 0.6$) were similar across Braak α -synuclein stages. Age was significantly different across Braak α -synuclein stages ($p = 0.003$), and post-hoc analyses revealed that donors at Braak stage 3 were older than donors at Braak stage 6 (87 ± 7 vs 75 ± 7 years, $p = 0.022$). Compared to non-diseased controls, TH neuronal density was significantly lower in PD (-56% , $p < 0.001$), and not significantly lower in iLBD (-31% , $p = 0.424$) (Supplementary Fig. 7). LB density in the substantia nigra (SN), anterior cingulate cortex (ACC) and prefrontal cortex (PFC) is shown in Supplementary Fig. 7.

Severe dopaminergic denervation in PD but not in iLBD

DAT, VGLUT1 and PSD95 synapses were quantified in putamen of all donors (Fig. 1). DAT synaptic density in the putamen was 86% lower in PD compared to controls ($d = -5.23$, $p < 0.001$), 84% lower in PD compared to iLBD (-84% , $d = -4.79$, $p < 0.001$), and similar in iLBD compared to controls (-13% , $p = 0.333$) (Fig. 1A, B). Across Braak α -synuclein stages, DAT synaptic density was significantly lower in Braak stage 4–6 compared to controls (Braak 4: -40% , $d = -2.10$, $p < 0.001$; Braak 5: -81% , $d = -4.69$, $p < 0.001$; Braak 6: -83% , $d = -5.27$, $p < 0.001$),

Table 1 | Demographics and pathological scores of donors in the study cohort

| Parameters | Control | iLBD | PD | p value |
|---|-------------------|-------------------------------|--------------------|------------|
| N (tot = 69) | 10 | 32 | 27 | |
| Sex F/M (%F) | 4/6 (40%) | 20/12* (63%) | 7/20 (26%) | 0.015* |
| Age at death years; mean [range] | 76 [67, 85] | 85 ^{##, **} [66, 96] | 77 [56, 92] | < 0.001*** |
| Disease duration years; mean [range] | – | – | 16 [8, 28] | |
| PMD h:min Mean [range] | 6:35 [3:50, 8:45] | 6:35 [4:25, 11:45] | 6:30 [3:30, 10:10] | 0.3 |
| Braak α-syn stage¹⁰ N (%) | | | | – |
| 0 | 10 (100%) | 0 (0%) | 0 (0%) | |
| 1 | 0 (0%) | 10 (31%) | 0 (0%) | |
| 2 | 0 (0%) | 3 (9.4%) | 0 (0%) | |
| 3 | 0 (0%) | 9 (28%) | 0 (0%) | |
| 4 | 0 (0%) | 7 (22%) | 5 (19%) | |
| 5 | 0 (0%) | 2 (6.3%) | 12 (44%) | |
| 6 | 0 (0%) | 1 (3.1%) | 10 (37%) | |
| Braak NFT stage⁷⁰ N (%) | | | | 0.14 |
| B0 | 2 (20%) | 1 (3.1%) | 1 (3.7%) | |
| B1 | 5 (50%) | 21 (66%) | 22 (81%) | |
| B2 | 3 (30%) | 10 (31%) | 4 (15%) | |
| B3 | 0 (0%) | 0 (0%) | 0 (0%) | |
| Thal phase⁷⁰ N (%) | | | | 0.3 |
| A0 | 2 (20%) | 5 (16%) | 6 (22%) | |
| A1 | 8 (80%) | 19 (59%) | 12 (44%) | |
| A2 | 0 (0%) | 7 (22%) | 9 (33%) | |
| A3 | 0 (0%) | 1 (3.1%) | 0 (0%) | |

Data are the mean and range. Group comparison: $p < 0.01^*$, $p < 0.001^{***}$. Post-hoc: $p < 0.01^{**}$ compared to controls; $p < 0.05^*$, $p < 0.01^{**}$ compared to PD (Mann–Whitney U-test for continuous data and Fisher exact test for categorical data). α -syn α -synuclein, F female, iLBD incidental Lewy body disease, M male, NFT neurofibrillary tangles, PD Parkinson's disease, PMD post-mortem delay, tot total.

Table 2 | Donor's characteristics across Braak α -synuclein stages

| Braak α -syn stage ¹⁰ | Controls | Braak 1 | Braak 2 | Braak 3 | Braak 4 | Braak 5 | Braak 6 | p value |
|---|-------------------|-------------------|-------------------|--------------------|--------------------|-------------------|-------------------|---------|
| N | 10 | 10 | 3 | 9 | 12 | 14 | 11 | |
| Clinical PD N (% clinical PD) | 0 (0%) | 0 (0%) | 0 (0%) | 0 (0%) | 5 (42%) | 12 (86%) | 10 (91%) | |
| Age at death years; mean [range] | 76 [67, 85] | 85 [66, 95] | 81 [77, 86] | 87 [72, 95] | 84 [68, 96] | 78 [56, 88] | 75 [62, 86] | 0.003 |
| Sex F/M (%F) | 4/6 (40%) | 5/5 (50%) | 3/0 (100%) | 5/4 (56%) | 6/6 (50%) | 4/10 (29%) | 4/7 (36%) | 0.4 |
| PMD h:min mean [range] | 6:35 [3:50, 8:45] | 6:25 [4:25, 10:0] | 6:40 [4:35, 6:55] | 7:15 [4:50, 11:45] | 6:40 [4:20, 10:10] | 5:55 [4:10, 9:15] | 6:40 [3:30, 9:25] | 0.4 |
| Thal phase⁷⁰ N (%) | | | | | | | | 0.11 |
| A0 | 2 (20%) | 2 (20%) | 0 (0%) | 2 (22%) | 1 (8%) | 6 (43%) | 0 (0%) | |
| A1 | 8 (80%) | 6 (60%) | 2 (67%) | 5 (56%) | 6 (50%) | 5 (36%) | 7 (64%) | |
| A2 | 0 (0%) | 2 (20%) | 0 (0%) | 2 (22%) | 5 (42%) | 3 (21%) | 4 (36%) | |
| A3 | 0 (0%) | 0 (0%) | 1 (33%) | 0 (0%) | 0 (0%) | 0 (0%) | 0 (0%) | |
| Braak NFT stage⁷⁰ N (%) | | | | | | | | 0.6 |
| B0 | 2 (20%) | 1 (10%) | 0 (0%) | 0 (0%) | 0 (0%) | 1 (7%) | 0 (0%) | |
| B1 | 5 (50%) | 6 (60%) | 3 (100%) | 6 (67%) | 9 (75%) | 11 (79%) | 9 (82%) | |
| B2 | 3 (30%) | 3 (30%) | 0 (0%) | 3 (33%) | 3 (25%) | 2 (14%) | 2 (18%) | |
| B3 | 0 (0%) | 0 (0%) | 0 (0%) | 0 (0%) | 0 (0%) | 0 (0%) | 0 (0%) | |

Data are the mean and range.

α -syn α -synuclein, F female, M male, NFT neurofibrillary tangles, PD Parkinson's disease, PMD post-mortem delay.

and similar to controls in Braak stages 1-3 (Braak 1: -9% , $p = 0.399$; Braak 2: -10% , $p = 0.452$; Braak 3: -9% , $p = 0.362$) (Fig. 1C). To explore whether DAT denervation was PD specific in late Braak α -synuclein stages, we separated iLBD and PD cases across Braak α -synuclein stages 4-6. PD cases showed severe DAT loss compared to controls (Braak 4: -74% , $p < 0.001$; Braak 5: -86% , $p < 0.001$; Braak 6: -92% , $p < 0.001$). Regarding iLBD cases with Braak α -synuclein stages 4-6, only 1 out of the 8 iLBD cases in this group showed DAT synaptic loss at Braak stage 5 (case number 45 in Supplementary Table 1). Decreased DAT synaptic density strongly correlated with higher Braak α -synuclein stage ($r_s = -0.77$, $R^2 = 60\%$, $p < 0.001$). The density of VGLUT1 (PD vs controls: $p = 0.694$; iLBD vs controls: $p = 0.150$) and PSD95 synapses (PD vs controls: $p = 0.509$; iLBD vs controls: $p = 0.519$) was similar between control, iLBD and PD groups (Fig. 1F, G), and across Braak α -synuclein stages (all $p > 0.05$). Sex had a significant effect on DAT synaptic density ($p = 0.045$), likely due to the predominance of males in the PD group, but no effect on VGLUT1 ($p = 0.281$) or PSD95 synaptic density ($p = 0.682$). Age had no significant effect on any of the synaptic densities (all $p > 0.05$).

Taken together, PD cases showed severe dopaminergic denervation in the putamen starting from Braak α -synuclein stage 4, while iLBD cases did not show dopaminergic denervation. Cortical glutamatergic and post-synaptic terminals remained unaffected in both iLBD and PD.

Enrichment of α -synuclein proteoforms in synaptic terminals

First, we investigated whether α -synuclein proteoforms are enriched in DAT, VGLUT1 and PSD95 synapses of control, iLBD and PD donors. See Supplementary Figs. 8 and 9 for representative images of single (Supplementary Fig. 8) and co-localised (Supplementary Fig. 9) α -synuclein proteoforms immunoreactivity in control, iLBD and PD putamen.

Syn1 α -synuclein⁺ synapses. Syn1 α -synuclein⁺ DAT synaptic density was 86% lower in PD compared to both controls ($d = -1.28$, $p = 0.008$) and iLBD ($d = -1.29$, $p = 0.001$), whereas it was similar between iLBD and controls ($p = 0.999$). Syn1 α -synuclein⁺ VGLUT1 and PSD95 synaptic density did not differ between groups (VGLUT1: PD vs controls: $p = 0.897$; iLBD vs controls: $p = 0.659$; PSD95: PD vs controls: $p = 0.561$; iLBD vs controls: $p = 0.611$) (Fig. 2A-C). DAT, VGLUT1 and

PSD95 synaptic density positive to Syn1 α -synuclein clusters⁺ (defined as spots of high-intensity and high-contrast compared to the background, resembling pathological α -synuclein clusters) was similar between groups (all $p > 0.05$; Supplementary Fig. 10).

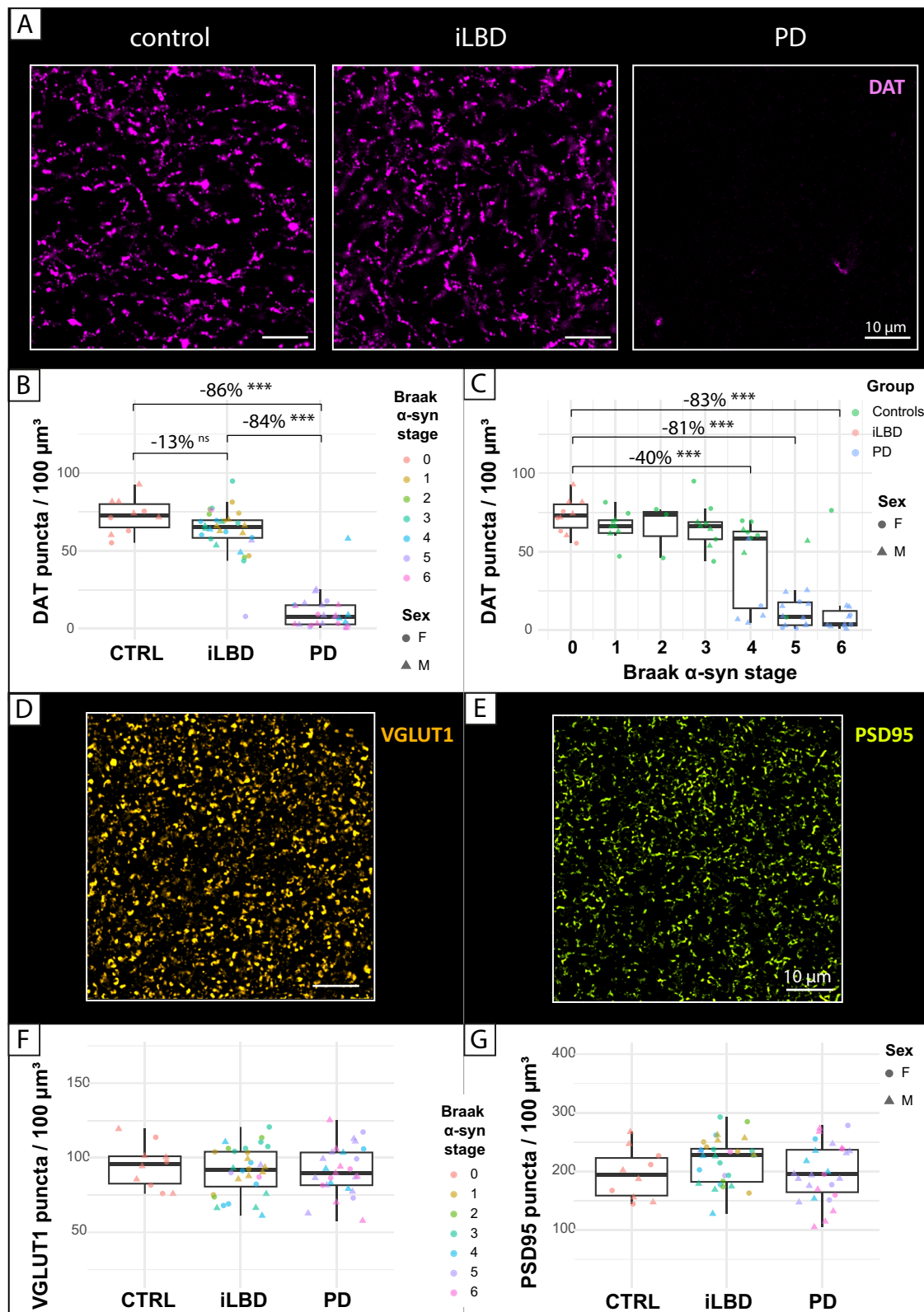
pSer129 α -synuclein⁺ synapses. pSer129 α -synuclein⁺ DAT synaptic density tended to be higher by 1253% in PD compared to controls ($d = 0.70$, $p = 0.064$), and was similar between iLBD and controls ($p = 0.159$). pSer129 α -synuclein⁺ VGLUT1 synaptic density was 1030% higher in PD compared to controls ($d = 1.80$, $p < 0.001$) and 280% higher in PD compared to iLBD ($d = 1.55$, $p < 0.001$), and was similar between iLBD and controls ($p = 0.787$). pSer129 α -synuclein⁺ PSD95 synaptic density was 877% higher in PD compared to controls ($d = 1.68$, $p < 0.001$) and +259% higher in PD compared to iLBD ($d = 1.35$, $p < 0.001$), and was similar between iLBD and controls ($p = 0.545$) (Fig. 2D-F). For colocalization images of pSer129 α -synuclein with synaptic puncta, see Supplementary Fig. 11.

CTT122 α -synuclein⁺ synapses. CTT122 α -synuclein⁺ DAT synaptic density did not differ between groups (all $p > 0.05$). CTT122 α -synuclein⁺ VGLUT1 synaptic density was 1022% higher in PD compared to controls ($d = 1.75$, $p = 0.001$) and 330% higher in PD compared to iLBD ($d = 1.27$, $p = 0.003$), and was similar between iLBD and controls ($p = 0.584$). CTT122 α -synuclein⁺ PSD95 synaptic density was 744% higher in PD compared to controls ($d = 1.99$, $p < 0.001$) and 270% higher in PD compared to iLBD ($d = 1.40$, $p < 0.001$), and was similar between controls and iLBD ($p = 0.421$) (Fig. 2G-I). For colocalization images of pSer129 α -synuclein with synaptic puncta, see Supplementary Fig. 12.

Neither age nor sex had a significant effect on synaptic enrichment of α -synuclein proteoforms. Taken together, Syn1 α -synuclein⁺ DAT synaptic density was decreased, while pSer129 and CTT122 α -synuclein were enriched in synaptic terminals in the putamen of PD cases compared to controls. In iLBD, α -synuclein synaptic enrichment was between control and PD values, but did not differ compared to controls.

Early enrichment of pSer129 α -synuclein in DAT synapses

Next, we investigated at which Braak α -synuclein stage α -synuclein proteoforms are enriched in DAT, VGLUT1 and PSD95 synapses,



their synaptic size, and if they are found within synaptic pairs. Synaptic pairs are defined as DAT⁺ and VGLUT1⁺ puncta next to a PSD95⁺ synapse ($\leq 1 \mu\text{m}$; see “Methods” for details).

Syn1 α -synuclein⁺ synapses. Syn1 α -synuclein⁺ DAT synaptic density tended to be lower at Braak stage 5 (-72% , $d = -1.03$, $p = 0.051$) and 6 (-68% , $d = -0.97$, $p = 0.077$) compared to controls, and it was similar

across Braak stages 1-4 (all $p > 0.05$). Syn1 α -synuclein⁺ VGLUT1 ($p > 0.05$) and PSD95 ($p > 0.05$) synaptic density did not change across Braak α -synuclein stages (Fig. 3A and Supplementary Fig. 13A–C).

pSer129 α -synuclein⁺ synapses. pSer129 α -synuclein⁺ DAT synaptic density was significantly higher at Braak stage 3 ($+2000\%$, $d = 1.07$, $p = 0.007$), 4 ($+1269\%$, $d = 0.74$, $p = 0.036$), and 5 ($+1613\%$, $d = 0.92$,

Fig. 1 | Putaminal DAT, VGLUT1 and PSD95 synaptic density in controls, iLBD, and PD. **A** Representative image of DAT synaptic density in the putamen of control, iLBD (Braak stage 3), and PD (Braak stage 6) (case numbers 9, 30, and 65 in Supplementary Table 1, respectively). **B** Quantification of DAT synaptic density per group. **C** Quantification of DAT synaptic density per Braak α -synuclein stage. **D, E** Show representative images of VGLUT1 and PSD95 synaptic density, respectively, in the putamen of a control. **F, G** Show the quantification of VGLUT1 and PSD95 synaptic density per group. Data points are average per case (average of all 6 ROIs), are shape-coded for sex, and are colour-coded per Braak α -synuclein stage in (**B, F**, and **G**) and per group in (**C**). Boxplots display the median (central line), the first and third quartiles (box hinges at the 25th and 75th percentiles), and whiskers that extend to the most extreme data points within 1.5 times the interquartile range

$p = 0.006$) compared to controls, and did not differ at Braak stage 1 ($p = 0.690$), 2 ($p = 0.945$), and 6 ($p = 0.121$). pSer129 α -synuclein⁺ VGLUT1 synaptic density was significantly higher at Braak stage 5 (+854%, $d = 1.53$, $p < 0.001$), and 6 (+1365%, $d = 2.20$, $p < 0.001$) compared to controls, and did not differ at Braak stages 1–4 (all $p > 0.05$). pSer129 α -synuclein⁺ PSD95 synaptic density tended to be higher at Braak stage 4 (+263%, $d = 0.58$, $p = 0.098$) and was significantly higher at Braak stage 5 (+785%, $d = 1.58$, $p < 0.001$), and 6 (+1103%, $d = 1.92$, $p < 0.001$) compared to controls, and did not differ at Braak stage 1–3 (all $p > 0.05$) (Fig. 3B and Supplementary Fig. 13D–F).

CTT122 α -synuclein⁺ synapses. CTT122 α -synuclein⁺ DAT synaptic density tended to be higher at Braak stage 4 (+294%, $d = 0.69$, $p = 0.061$) and was significantly higher at Braak stage 6 (+437%, $d = 0.92$, $p = 0.012$) compared to controls, and did not differ at Braak stages 1–3 and 5 (all $p > 0.05$). CTT122 α -synuclein⁺ VGLUT1 synaptic density was significantly higher at Braak stage 5 (+405%, $d = 1.03$, $p = 0.031$), and 6 (+1920%, $d = 2.72$, $p < 0.001$) compared to controls, and did not differ at Braak stage 1–4 (all $p > 0.05$). CTT122 α -synuclein⁺ PSD95 synaptic density tended to be higher at Braak stage 4 (+219%, $d = 0.93$, $p = 0.061$) and was significantly higher at Braak stage 5 (+337%, $d = 1.35$, $p = 0.004$), and 6 (+1332%, $d = 2.87$, $p < 0.001$) compared to controls, and did not differ at Braak stage 1–3 (all $p > 0.05$) (Fig. 3C and Supplementary Fig. 13G–I).

α -Synuclein⁺ synapses: size and synaptic pairs. pSer129 and CTT122 α -synuclein⁺ VGLUT1 synapses were significantly larger (swollen) in iLBD (CTT122: +14%, $d = 1.00$, $p = 0.008$) and PD (pSer129: +5%, $d = 0.34$, $p = 0.001$; CTT122: +23%, $d = 1.65$, $p < 0.001$) compared to controls. Interestingly, control VGLUT1 synapses were smaller when positive for CTT122 α -synuclein (−18%, $d = 0.38$, $p < 0.001$). pSer129 and CTT122 α -synuclein was enriched almost exclusively in synaptic pairs (pSer129, DAT: 99.4%, $d = 9.71$, $p < 0.001$; pSer129, VGLUT1: 96.1%, $d = 4.54$, $p < 0.001$; CTT122, DAT: 99.1%, $d = 7.91$, $p < 0.001$; CTT122, VGLUT1: 98.7%, $d = 5.47$, $p < 0.001$) (Supplementary Fig. 14; for results on Syn1 α -synuclein clusters⁺ synapses see Supplementary Fig. 15).

Taken together, pSer129 was the earliest α -synuclein proteoform found to be enriched in synapses. pSer129 α -synuclein appeared enriched already at Braak stage 3 in dopaminergic synapses, while CTT122 α -synuclein was enriched in later stages. In cortical glutamatergic and post-synapses, both pSer129 and CTT122 α -synuclein showed enrichment in the putamen at Braak stage 5–6. In contrast, Syn1 α -synuclein dopaminergic density was lower at Braak stages 5 and 6. All pre-synapses that showed enrichment of pSer129 and CTT122 α -synuclein were almost exclusively found within synaptic pairs, i.e. next to a post-synapse. In addition, glutamatergic synapses enriched in pSer129 and CTT122 α -synuclein were swollen.

Syn1 α -synuclein⁺ DAT synaptic density is decreased and reflects DAT synaptic loss in PD

As the effect size of Syn1 α -synuclein⁺ DAT synaptic density loss was very similar to DAT synaptic loss in PD ($\approx 86\%$), and since Syn1 α -

from the hinges. The sample consists of $n = 69$ (control = 10, iLBD = 32, PD = 27), and six technical replicates are averaged for each brain donor. The statistical test used is a two-sided LMM with age and sex as covariates, and nested for dataset and case ID. Multiple pairwise (post-hoc) and multiple testing comparison corrections were performed with the Tukey test. Exact p values: **B** control vs PD $p < 0.001$, iLBD vs PD $p < 0.001$, control vs iLBD $p = 0.334$; **C** control vs Braak 4 $p < 0.001$, control vs Braak 5 $p < 0.001$, control vs Braak 6 $p < 0.001$; **F, G** all $p > 0.05$. Source data are provided as a Source Data file. CTRL control, DAT dopaminergic transporter, iLBD incidental Lewy body disease, PD Parkinson's disease, PSD95 post-synaptic density 95, VGLUT1 vesicular glutamatergic transporter 1, ns non-significant; $p < 0.05$, $p < 0.01$, $p < 0.001$.

synuclein was specifically decreased in DAT synapses, we addressed whether the decrease in Syn1 α -synuclein-positive DAT synaptic density reflected DAT synaptic loss. We found a strong positive correlation between Syn1 α -synuclein⁺ DAT synaptic density and DAT synaptic density across all cases ($\rho = 0.61$, $R^2 = 38\%$, $p < 0.001$), suggesting that the decrease in Syn1 α -synuclein⁺ DAT synaptic density reflected DAT denervation (Fig. 4A).

α -Synuclein enrichment in DAT synapses is linked to DAT loss

As DAT synapses were enriched in both pSer129 and CTT122 α -synuclein at different Braak stages, we wondered whether this observation was associated with DAT synaptic loss. To answer this question, we correlated DAT synaptic density with the percentage (to correct for DAT loss) of DAT synapses positive for pSer129 and CTT122 α -synuclein across all cases, and within iLBD and PD groups. We found a strong negative correlation between DAT synaptic density and percentage of DAT synapses positive for pSer129 α -synuclein across all cases ($\rho = -0.54$, $R^2 = 30\%$, $p < 0.001$), which was driven by the iLBD group ($\rho = -0.51$, $R^2 = 26\%$, $p = 0.002$), and was non-significant in PD ($p = 0.905$), probably suffering a floor-effect due to almost complete DAT denervation in this group (Fig. 4B). Similarly, we found a moderate negative correlation between DAT synaptic density and percentage of DAT synapses positive for CTT122 α -synuclein across all cases ($\rho = -0.47$, $R^2 = 22\%$, $p < 0.001$), which was again driven by the iLBD group ($\rho = -0.31$, $R^2 = 10\%$, $p < 0.001$), and was non-significant in PD ($p = 0.493$) (Fig. 4C).

In summary, the increase of pSer129 and CTT122 α -synuclein enrichment in DAT synapses is associated with DAT denervation, especially in iLBD.

α -Synuclein enrichment in VGLUT1 terminals prior to cortical LBs

Since DAT synapses in the putamen are the pre-synaptic terminals of dopaminergic neurons found in the SN, we investigated the correlation between pSer129 and CTT122 α -synuclein enrichment in putaminal DAT synapses and LB density in the SN. The density of both pSer129 ($\rho = 0.42$, $R^2 = 18\%$, $p < 0.001$, Fig. 5A, D) and CTT122 ($\rho = 0.35$, $R^2 = 12\%$, $p = 0.035$, Fig. 5G, J) α -synuclein⁺ DAT synaptic density positively correlated with LB density in the SN, suggesting that with more dopaminergic terminals positive for α -synuclein, there were more LBs in dopaminergic neurons in the SN.

Since VGLUT1 synapses correspond to the glutamatergic pre-synaptic terminals of corticostriatal projection neurons found in the cortex^{25,26}, we investigated the correlation between α -synuclein proteoform enrichment in VGLUT1 synapses in the areas of the putamen innervated by the ACC and the PFC²⁷, and LB density in ACC and the PFC, respectively. The density of both pSer129 (ACC: $\rho = 0.71$, $R^2 = 50\%$, $p < 0.001$; PFC: $\rho = 0.54$, $R^2 = 30\%$, $p < 0.001$, Fig. 5B, C) and CTT122 (ACC: $\rho = 0.71$, $R^2 = 50\%$, $p < 0.001$; PFC: $\rho = 0.74$, $R^2 = 55\%$, $p < 0.001$, Fig. 5H, I) α -synuclein⁺ VGLUT1 synapses in the ACC and PFC innervation region of the putamen positively correlated with LB density in the ACC and PFC, respectively. Interestingly, pSer129 α -synuclein was significantly

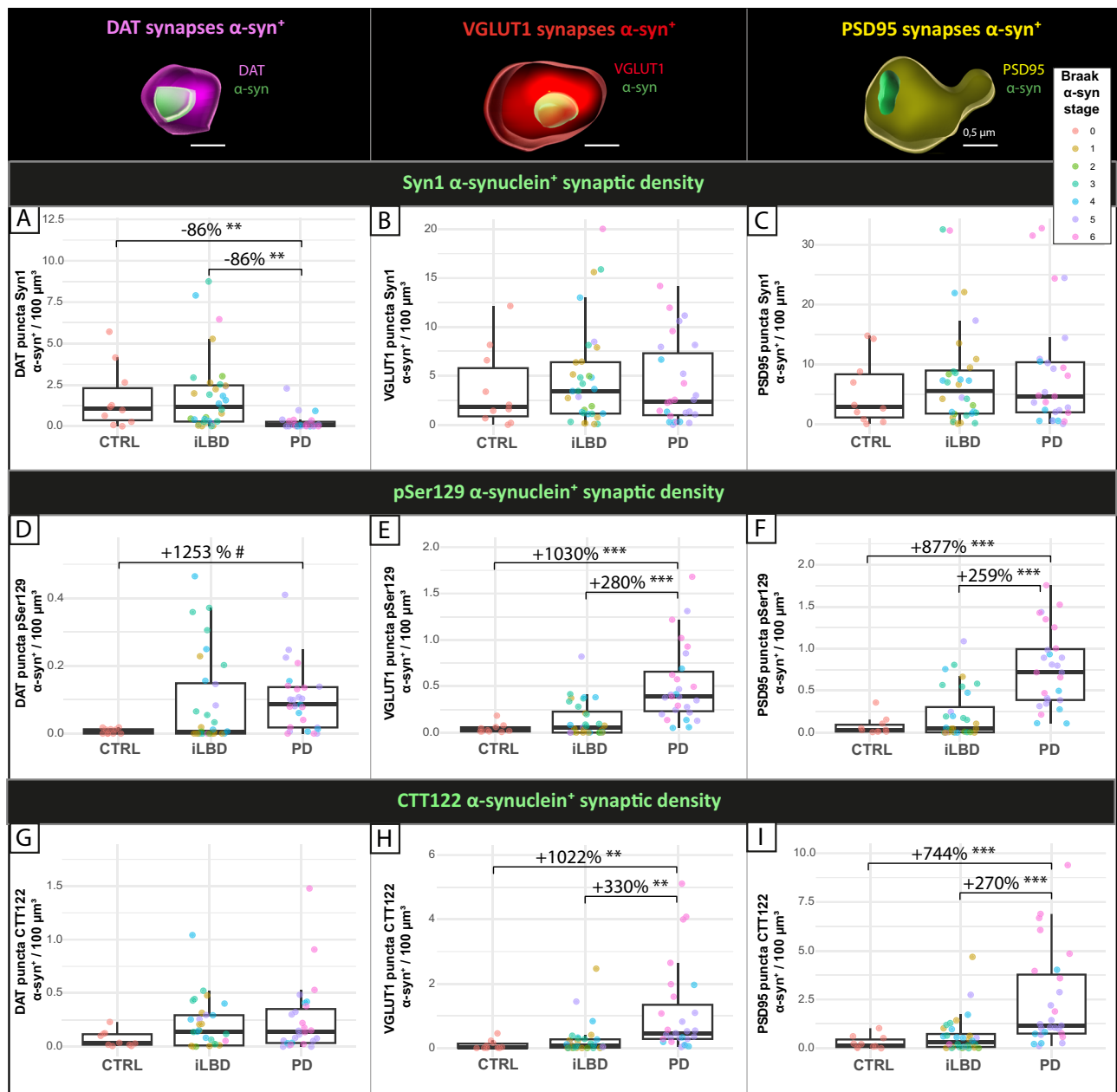


Fig. 2 | α -Synuclein proteoforms in putaminal DAT, VGLUT1 and PSD95 synapses in control, iLBD and PD. **A** Syn1 α -synuclein⁺ DAT synaptic density was decreased specifically in the PD group, while Syn1 α -synuclein⁺. **B** VGLUT1 and **C** PSD95 synaptic density did not change between groups. pSer129 α -synuclein⁺ synaptic density tended to be higher in **(D)** DAT synapses, and it was higher in **(E)** VGLUT1, and **F** PSD95 synapses in PD. **G** CTT122 α -synuclein⁺ DAT synaptic density did not differ between groups, while CTT122 α -synuclein⁺, **H** VGLUT1, and **I** PSD95 synaptic density were higher in PD. Data points are average per case (average of all 6 ROIs), and are colour-coded per Braak α -synuclein stage. Boxplots display the median (central line), the first and third quartiles (box hinges at the 25th and 75th percentiles), and whiskers that extend to the most extreme data points within 1.5 times the interquartile range from the hinges. On top, a representative 3D surface-rendering image of DAT (magenta), VGLUT1 (red), and PSD95 (yellow) synapses positive for α -synuclein proteoforms (green) is shown (scale bar 0.5 μ m). The sample consists of $n = 69$ (control = 10, iLBD = 32, PD = 27),

and 6 technical replicates are averaged for each brain donor. The statistical test used is a two-sided LMM with age and sex as covariates, and nested for case ID. Multiple pairwise (post-hoc) and multiple testing comparison corrections were performed with the Tukey test. Exact p values: **A** control vs PD $p = 0.008$, iLBD vs PD $p = 0.001$, control vs iLBD $p = 0.999$; **B, C**: all $p > 0.05$; **D**: control vs PD $p = 0.064$, iLBD vs PD $p = 0.909$, control vs iLBD $p = 0.159$; **E**: control vs PD $p < 0.001$, iLBD vs PD $p < 0.001$, control vs iLBD $p = 0.787$; **F** control vs PD $p < 0.001$, iLBD vs PD $p < 0.001$, control vs iLBD $p = 0.545$; **G**: all $p > 0.05$; **H**: control vs PD $p = 0.001$, iLBD vs PD $p = 0.003$, control vs iLBD $p = 0.584$; **I**: control vs PD $p < 0.001$, iLBD vs PD $p < 0.001$, control vs iLBD $p = 0.521$. Source data are provided as a Source Data file. α -syn α -synuclein, CTRL control, DAT dopaminergic transporter, iLBD incidental Lewy body disease, PD Parkinson's disease, PSD95 post-synaptic density 95, VGLUT1 vesicular glutamatergic transporter 1. $0.10 < p \leq 0.05^{\#}$, $p < 0.05^*$, $p < 0.01^{**}$, $p < 0.001^{***}$.

enriched in VGLUT1 synapses in the ACC and PFC innervation regions of the putamen already at Braak α -synuclein stage 3 (ACC: $p = 0.003$; PFC: $p = 0.008$) and 4 (ACC: $d = p = 0.035$; PFC: $p = 0.002$) compared to LB density in connected cortical regions (Fig. 5E, F),

which per definition show LBs only from Braak α -synuclein stage 5¹⁰. Similarly, CTT122 α -synuclein was significantly enriched in VGLUT1 pre-synaptic terminals at Braak α -synuclein stage 3 (ACC: $p = 0.003$; PFC: $p = 0.004$, Fig. 5K, L).

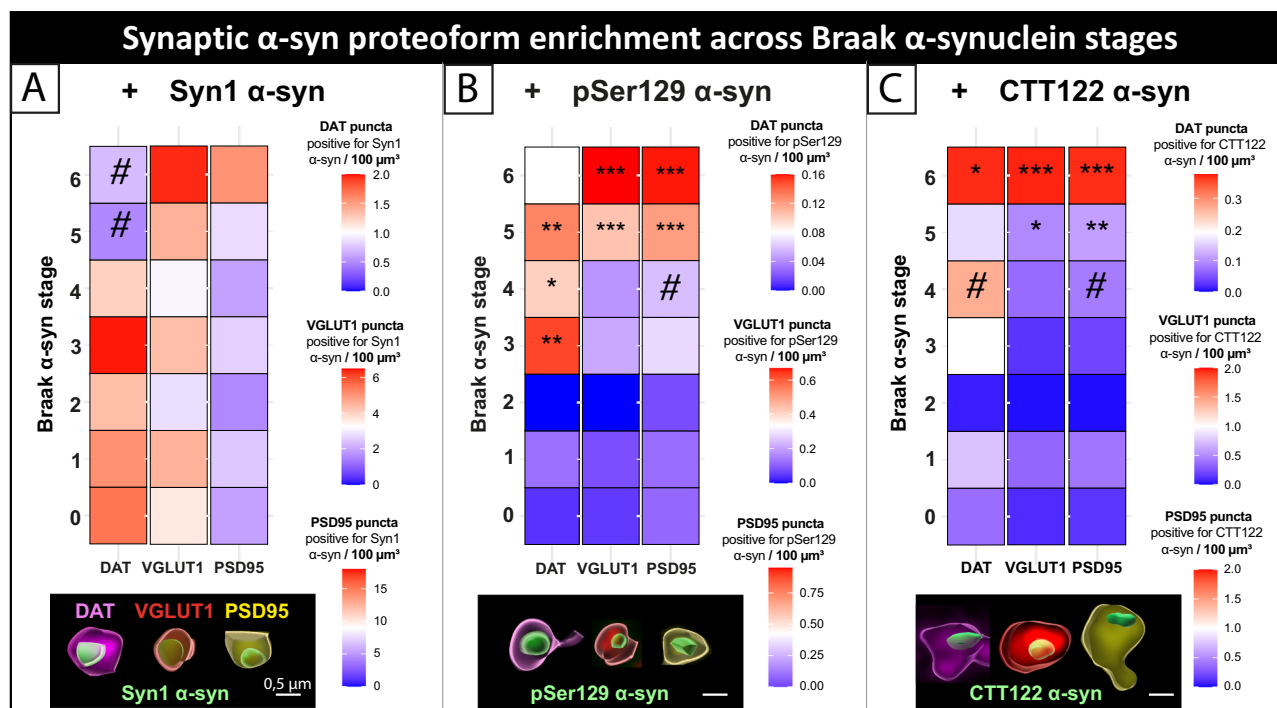


Fig. 3 | Stage-dependent α -synuclein proteoform enrichment in putamenal DAT, VGLUT1 and PSD95 synapses across Braak α -synuclein stages. **A** Syn1 α -synuclein, **B** pSer129 α -synuclein, and **C** CTT122 α -synuclein enrichment in DAT, VGLUT1, and PSD95 synapses in the putamen across Braak α -synuclein stages (on y axis, 0 is controls) is shown. Heat maps are colour-coded for the average density of synapses positive for α -synuclein proteoforms per Braak stage (first averaged per case across all 6 ROIs, and then per Braak α -synuclein stage group), with values similar to zero in blue, high values in red, and mid values in white. Each heatmap column has its own legend, located on the right of the corresponding panel (e.g. the DAT column legend in the Syn1 panel is on the top right of the panel). Units in heatmap legends are expressed as the density of puncta positive for α -synuclein proteoforms per $100 \mu\text{m}^3$. Below each heatmap column, a representative 3D surface-rendering image of DAT (magenta), VGLUT1 (red), and PSD95 (yellow) synapses positive for α -synuclein proteoforms (green) is shown (scale bar $0.5 \mu\text{m}$). For all data points, see Supplementary Fig. 13. The Statistical test used is a two-sided LMM with age and sex as covariates, and nested for case ID. Multiple pairwise (post-

hoc) and multiple testing comparison corrections were performed with the Tukey test. Exact p values: **A** DAT: control vs Braak 1–4 all $p > 0.05$, control vs Braak 5 $p = 0.051$, control vs Braak 6 $p = 0.077$; **A** VGLUT1 and PSD95: control vs Braak 1–6 all $p > 0.05$, **B** DAT: control vs Braak 1–2 all $p > 0.05$, control vs Braak 3 $p = 0.007$, control vs Braak 4 $p = 0.036$, control vs Braak 5 $p = 0.006$, control vs Braak 6 $p = 0.121$; **B** VGLUT1: control vs Braak 1–4 all $p > 0.05$, control vs Braak 5 $p < 0.001$, control vs Braak 6 $p < 0.001$; **B** PSD95: control vs Braak 1–3 all $p > 0.05$, control vs Braak 4 $p = 0.098$, control vs Braak 5 $p < 0.001$, control vs Braak 6 $p < 0.001$; **C** DAT: control vs Braak 1–3 and 5 all $p > 0.05$, control vs Braak 4 $p = 0.061$, control vs Braak 6 $p = 0.012$; **C** VGLUT1: control vs Braak 1–4 all $p > 0.05$, control vs Braak 5 $p = 0.031$, control vs Braak 6 $p < 0.001$; **C** PSD95: control vs Braak 1–3 all $p > 0.05$, control vs Braak 4 $p = 0.061$, control vs Braak 5 $p = 0.004$, control vs Braak 6 $p < 0.001$. Source data are provided as a Source Data file. α -syn α -synuclein, DAT dopaminergic transporter, PSD95 post-synaptic density 95, VGLUT1 vesicular glutamatergic transporter 1. $0.10 < p \leq 0.05^*$, $p < 0.05^*$, $p < 0.01^{**}$, $p < 0.001^{***}$.

Taken together, pSer129 and CTT122 α -synuclein are enriched in VGLUT1 pre-synaptic terminals prior to the appearance of LBs in corticostriatal projection neurons in ACC and PFC.

pSer129 α -synuclein is enriched in PD putamenal synaptosomes

Abundant pre- and post-synapses of about $0.3\text{--}1 \mu\text{m}$ in diameter (as described before in ref. 28) were clearly visible by confocal microscopy isolated in synaptosome fractions, suggesting successful isolation of synaptosomes from frozen human putamen (Fig. 6D). Synaptosomal fractions were also enriched in pre- and post-synaptic proteins compared to total homogenate and cytosolic fractions (Supplementary Fig. 16). Total protein of synaptosomal fractions ($3.68 \pm 2.42 \text{ mg/mL}$) did not differ between PD ($p = 0.597$) and iLBD ($p = 0.505$) compared to controls, or across Braak stages (all $p > 0.05$), indicating similar isolation conditions between groups.

Total α -synuclein. Total synaptosomal α -synuclein levels ($\mu\text{g}/\text{mg}$ total protein) tended to be higher in PD compared to controls ($+48\%$, $p = 0.073$), and were comparable to control levels in iLBD ($p = 0.339$) and across Braak stages (all $p > 0.05$) (Fig. 7A).

pSer129 α -synuclein. Synaptosomal pSer129 α -synuclein levels ($\mu\text{g}/\text{mg}$ total protein) were significantly higher in PD ($+134\%$, $p = 0.043$) and

in cases with Braak 6 compared to controls ($+251\%$, $p = 0.033$) (Fig. 7A). Synaptosomal pSer129 α -synuclein levels ($\mu\text{g}/\text{mg}$ total protein) in iLBD seemed to have a trend of increase based on visual inspection, but statistically were comparable to control levels ($p = 0.392$) (Fig. 7A). The pSer129 ratio over total α -synuclein ($\mu\text{g}/\mu\text{g}$ total α -synuclein) in synaptosomes was similar to controls in PD and iLBD (PD vs control: $p = 0.137$; iLBD vs control: $p = 0.179$). Across Braak stages, the synaptosomal pSer129 ratio over total α -synuclein ($\mu\text{g}/\mu\text{g}$ total α -synuclein) was significantly higher in cases with Braak stage 6 ($+133\%$, $p = 0.035$), and tended to be higher in cases with Braak stages 4 ($+76\%$, $p = 0.095$) and 5 ($+70\%$, $p = 0.090$) compared to control levels (Fig. 7B), suggesting increased α -synuclein phosphorylation at Ser129 in synaptosomes of cases with late disease stages compared to control phosphorylation levels.

CTT122 α -synuclein. Synaptosomal CTT122 α -synuclein levels ($\mu\text{g}/\text{mg}$ total protein) were similar across iLBD, PD and control groups (PD vs control: $p = 0.178$; iLBD vs control: $p = 0.530$), and Braak stages (all $p > 0.05$) (Fig. 7A). The synaptosomal CTT122 ratio over total α -synuclein ($\mu\text{g}/\mu\text{g}$ total α -synuclein) was similar across PD, iLBD, and control groups (PD vs control: $p = 0.410$; iLBD vs control: $p = 0.974$), and Braak stages (all $p > 0.05$) (Fig. 7B), suggesting no increase in C-terminal truncation at residue 122 in PD synaptosomes.

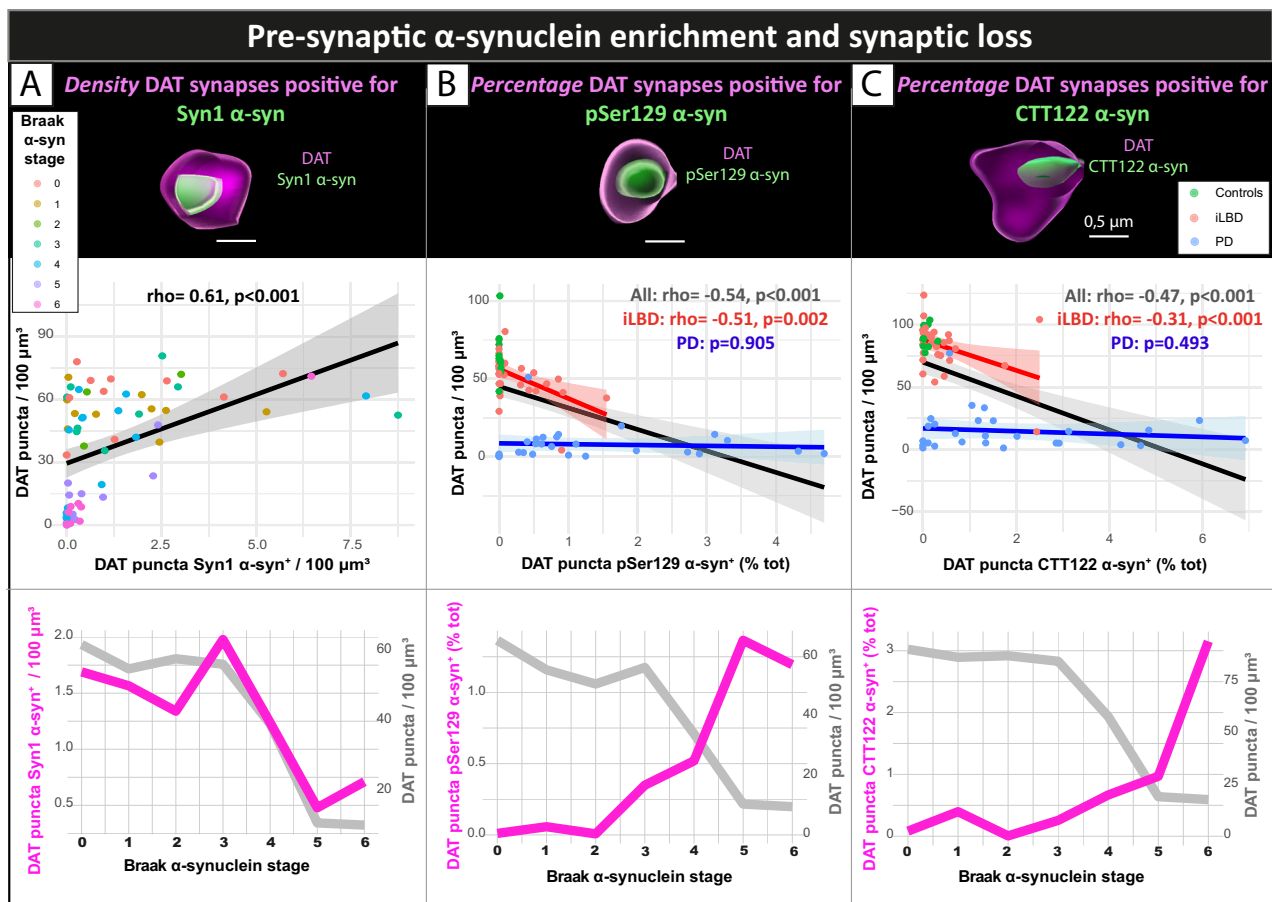


Fig. 4 | Relationship between α-synuclein enrichment in dopaminergic terminals and dopaminergic synaptic loss. **A** Syn1 α-synuclein, **B** pSer129 α-synuclein, and **C** CTT122 α-synuclein enrichment in DAT synapses is associated with DAT loss in the putamen across all cases. The *top row* shows a representative 3D surface-rendering image of DAT synapses (magenta) positive for α-synuclein proteoforms (green) (scale bar 0.5 μm). The *middle row* shows the correlation of **A** the density of Syn1 α-synuclein+ DAT synapses and DAT synaptic loss (data points are average per case across all 6 ROIs and colour-coded for Braak α-synuclein stage), **B** the percentage of DAT synapses positive for pSer129, and **C** CTT122 α-synuclein and DAT loss (data points are average per case across all 6 ROIs and colour-coded for group; black: regression line for all cases; red: regression line for iLBD cases; blue: regression line for PD cases; the grey area around the regression line represents the

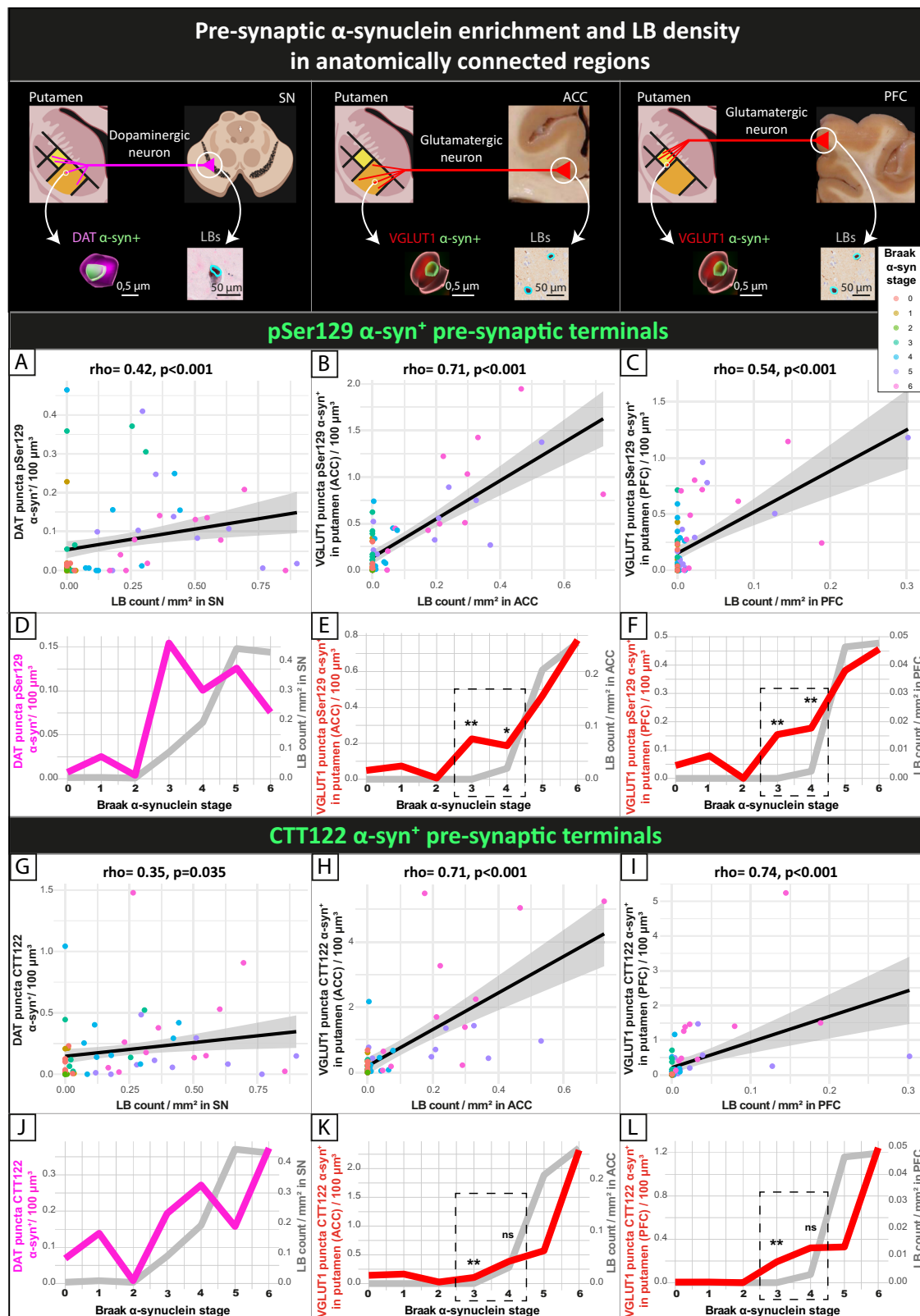
standard error). The *bottom row* shows the same correlation across Braak α-synuclein stages, where the grey line shows the mean DAT synaptic density (right y axis) and the magenta line the mean α-synuclein proteoform* DAT synaptic density/percentage (left y axis) per Braak α-synuclein stage (x axis). The statistical test used is a two-sided Spearman's correlation with age and sex as covariates. Multiple testing comparison corrections were performed with the Tukey test. Exact *p* values: **A**: all cases $\rho = 0.61, p < 0.001$; **B**: all cases $\rho = -0.54, p < 0.001$; iLBD $\rho = -0.51, p = 0.002$; PD $p = 0.905$; **C**: all cases $\rho = -0.47, p < 0.001$; iLBD $\rho = -0.31, p < 0.001$; PD $p = 0.493$. Source data are provided as a Source Data file. α-syn α-synuclein, DAT dopaminergic transporter, iLBD incidental Lewy body disease, PD Parkinson's disease, PSD95 post-synaptic density 95, VGLUT1 vesicular glutamatergic transporter 1. $0.10 < p \leq 0.05^*$, $p < 0.05^*$, $p < 0.01^{**}$, $p < 0.001^{***}$.

Comparison between α-synuclein PTMs levels. Both synaptosomal pSer129 and CTT122 α-synuclein (μg/mg total protein) strongly correlated with total α-synuclein levels (μg/mg total protein) ($\rho = 0.78, R^2 = 61\%, p < 0.001$; $\rho = 0.89, R^2 = 78\%, p < 0.001$ respectively), suggesting that these PTMs linearly increase with total α-synuclein levels in synaptosomes. Synaptosomal pSer129 and CTT122 α-synuclein levels (μg/mg total protein) also strongly correlated to each other ($\rho = 0.88, R^2 = 78\%, p < 0.001$) (Fig. 7C). However, the ratio of pSer129 and CTT122 levels over total α-synuclein levels in synaptosomes (μg/μg total α-synuclein) only moderately correlated to each other ($\rho = 0.48, R^2 = 23\%, p = 0.004$) (Fig. 7D), suggesting that phosphorylation at Ser129 and C-terminal truncation at residues 120–122 of α-synuclein only partially increase together in the synaptosomes of the same donors, with phosphorylation being more prominent than C-terminal truncation (average pSer129/CTT122 ratio 1.6, with peaks of 4.9).

Discussion

α-Synuclein is a presynaptic protein that plays an important role in synaptic transmission¹³. At the earliest stages of disease, its aggregation in pre-synaptic terminals in the striatum is hypothesised to set off

a cascade of events leading to synaptic loss and widespread cortical LB pathology. Here, based on microscopical and quantitative immuno-based analysis of the post-mortem human putamen, we report that: (i) enrichment of pSer129 α-synuclein in dopaminergic synapses is an early-event in PD, occurring prior to striatal dopaminergic denervation; (ii) enrichment of pSer129 and CTT122 α-synuclein in dopaminergic synapses contributes to dopaminergic, but not glutamatergic terminal loss; (iii) pSer129 and even more CTT122 contributes to synaptic swelling and may contribute to synaptic dysfunction; (iv) pSer129 and CTT122 α-synuclein enrichment in glutamatergic corticostriatal pre-synaptic terminals occurs prior to LB pathology in prefrontal and cingulate cortex; (v) reduction in synaptic Syn1 α-synuclein reflects dopaminergic terminal loss in the putamen; and (vi) total, pSer129 and CTT122 α-synuclein protein levels are quantifiable in putaminal synaptosomes in control, iLBD and PD brains with *in-house* developed AlphaLISA immunoassays. pSer129 α-synuclein protein levels were increased in putaminal synaptosomes in late-stage PD synaptosomes, but not in early stages. No changes in total or CTT122 α-synuclein protein levels could be detected in the synaptosomes across disease stages. These data strongly support the hypothesis that



pSer129 α -synuclein is enriched in striatal synaptic terminals early on in PD, possibly contributing to dopaminergic denervation and cortical LB pathology, while CTT122 α -synuclein enrichment in synaptic terminals accompanies pSer129 in later stages.

pSer129 α -synuclein is a major component of LBs^{20,29}, but it is still unclear what role it plays in the cellular metabolism of neurons³⁰. Under physiological conditions, only a small fraction of α -synuclein is

phosphorylated at Serine 129, while an enrichment of this PTM is consistently reported in the PD brain^{19,30}. Two recent studies^{31,32} have shown that physiological pSer129 α -synuclein can be found in small quantities in control pre-synapses, and that neuronal activity transiently augments its levels in vitro and in vivo. Our quantitative biochemical analysis also suggests that pSer129 α -synuclein is present in picogram levels in human control synaptosomal fractions, which

Fig. 5 | Relationship between pSer129 and CTT122 α -synuclein synaptic enrichment and LB density in anatomically connected regions. The top row illustrates the relationship between synaptic terminals in the putamen and their projection neurons in the SN and cortex. **A–L** illustrates the correlation of **A–F** pSer129 and **G–L** CTT122 α -synuclein positive synaptic terminals, and LB density in projection neurons in SN and cortex (data points in **A**, **G** are average per case across all six ROIs; data points in **B**, **H** are average per case across the four ROIs spanning the ACC innervation area of the putamen; data points in **C** and **I** are average per case across the two ROIs spanning the PFC innervation area of the putamen; all points are colour-coded for Braak α -synuclein stage; the grey area around the regression line represents the standard error). The grey line in **D–F** and **J–L** shows the mean LB density in the input region (right y axis), and the magenta (DAT) or red line (VGLUT1) shows the mean α -synuclein proteoform⁺ synaptic density in the putamen (left y axis) per Braak α -synuclein stage (x axis). Statistical

test used in **A–C** and **G–I** is a two-sided Spearman's correlation with age and sex as covariates. Exact p values: **A**: $\rho = 0.42$, $p < 0.001$; **B**: $\rho = 0.71$, $p < 0.001$; **C**: $\rho = 0.54$, $p < 0.001$; **G**: $\rho = 0.35$, $p = 0.035$; **H**: $\rho = 0.71$, $p < 0.001$; **I**: $\rho = 0.74$, $p < 0.001$. Statistical test used in **E**, **F**, **K**, and **L** is a two-sided LMM with age and sex as covariates, and nested for case ID, on the original log-transformed values that are scaled as a percentage (0–100%). Exact p values: **E**: Braak 3 $p = 0.003$, Braak 3 $p = 0.035$; **F**: Braak 3 $p = 0.008$, Braak 3 $p = 0.002$; **K**: Braak 3 $p = 0.003$, Braak 3 $p > 0.05$; **L**: Braak 3 $p = 0.004$, Braak 3 $p > 0.05$. Source data are provided as a Source Data file. Figure partially created in BioRender. Van de berg (2025) <https://BioRender.com/duygz72>. α -syn α -synuclein, ACC anterior cingulate cortex, DAT dopaminergic transporter, Lb Lewy body, PFC prefrontal cortex, PSD95 post-synaptic density 95, SN substantia nigra, VGLUT1 vesicular glutamatergic transporter 1. $0.10 < p \leq 0.05^*$, $p < 0.05^*$, $p < 0.01^{**}$, $p < 0.001^{***}$.

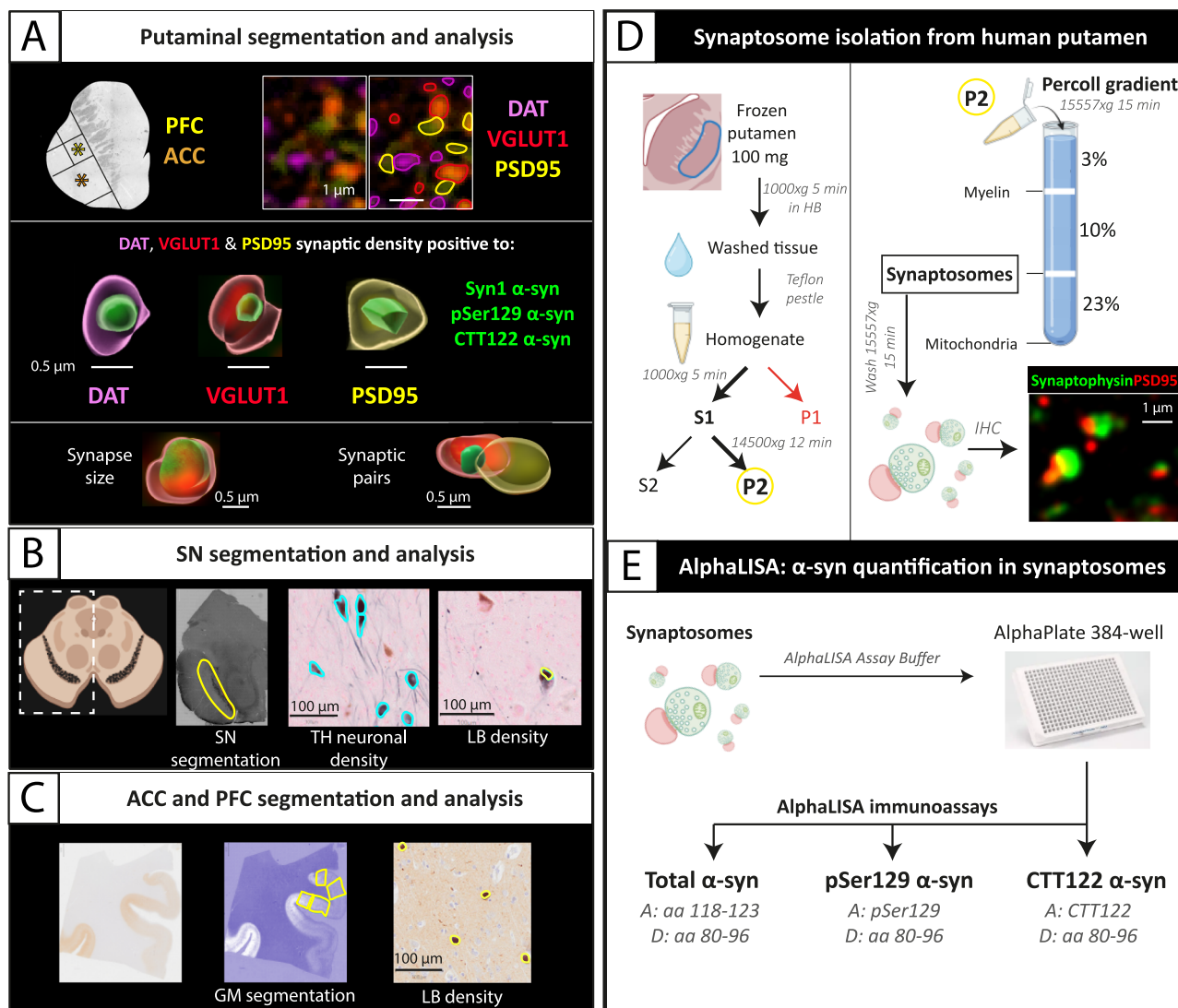
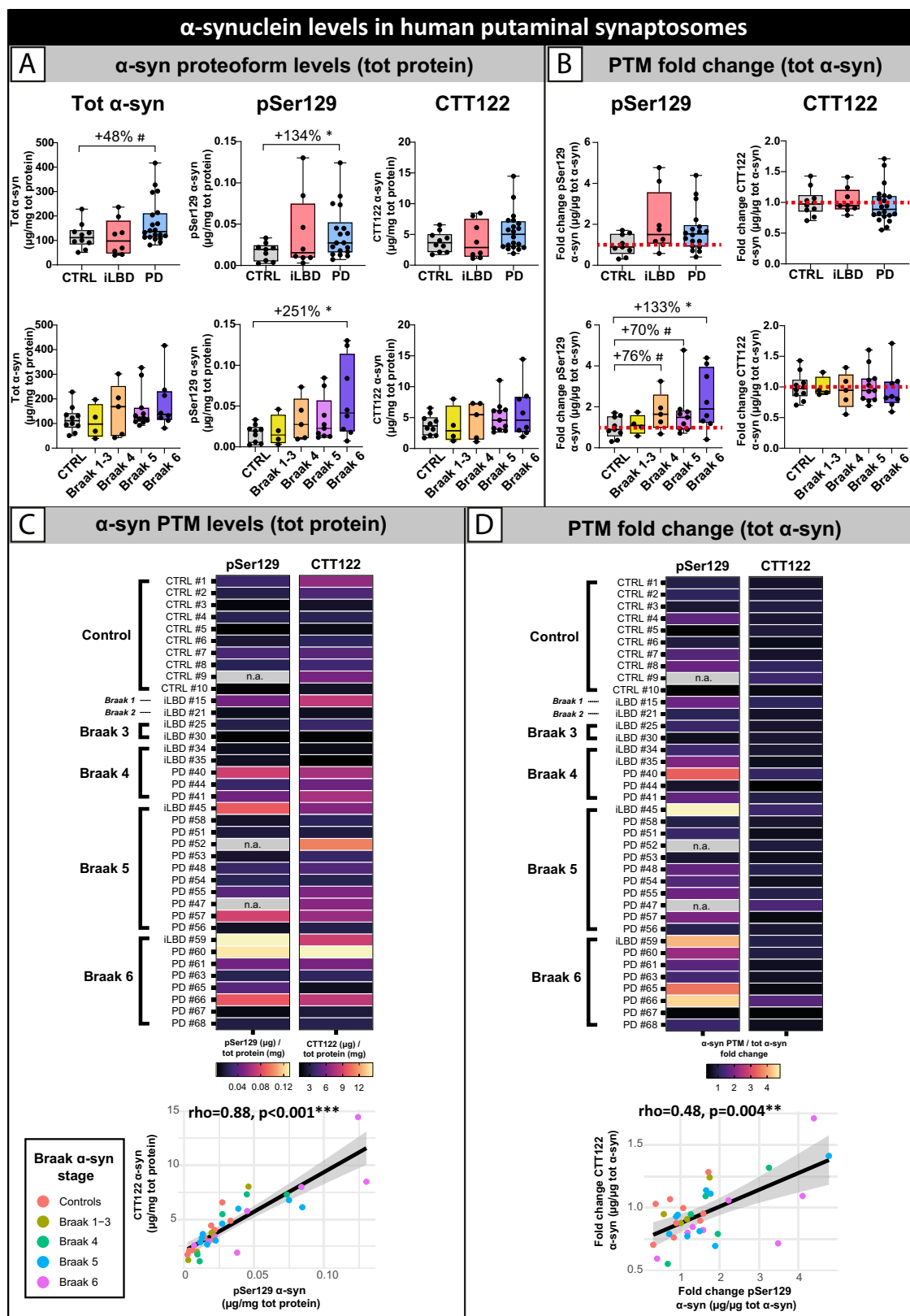


Fig. 6 | Methods workflow. **A** ROIs were placed in whole-slide scans of FFPE striatal sections. We selected ROIs in ACC- and PFC-innervated areas of the putamen (asterisks). DAT+, VGLUT1+, and PSD95+ synaptic density were quantified within the putaminal ROIs. The middle panel shows 3D reconstructions of DAT+, VGLUT1+, and PSD95+ synapses positive for different α -synuclein proteoforms. The bottom panel illustrates the quantification of synaptic size and synaptic pairs (pre- and post-synapse next to each other). **B** Dopaminergic neuronal density (TH+) and LB density were quantified in SN. **C** LB density was assessed in ACC and PFC. **D** Synaptosomes were isolated from frozen putamen in a subset of donors. **E** Total, pSer129, and CTT122 α -synuclein levels were quantified in synaptosome fractions

using AlphaLISA immunoassays. Figure partially created in BioRender. Van de berg (2025) <https://BioRender.com/6sljtqz>. α -syn α -synuclein, A coupled with acceptor bead, aa amino acids, ACC anterior cingulate cortex, CTT122 C-terminal truncated α -synuclein at amino acid 122, D coupled with donor bead, DAT dopamine transporter, GM grey matter, HB homogenization buffer, IHC immunohistochemistry, LB Lewy body, LH left hemisphere, PFC prefrontal cortex, PSD95 post-synaptic density 95, SN substantia nigra, pSer129 α -synuclein phosphorylated at Serine 129, Syn1 α -synuclein detected at amino acid 91–99, RH right hemisphere, Tyrosine hydroxylase TH, VGLUT1 vesicular glutamate transporter 1.



might be too low to be detected by common immunohistochemistry techniques. Importantly, our results add that pSer129 α -synuclein levels are increased (+134%) in PD putaminal synaptosomes, and that this enrichment specifically starts in dopaminergic pre-synapses in synaptic pairs (i.e. when dopaminergic synapses next to a post-synapse, where likely neuronal activity is present) early on at Braak stage 3. pSer129 α -synuclein positive aggregates have also been found

in pre- and post-synapses in putamen and anterior cingulate cortex of end-stage DLB donors²³, but whether excessive synaptic pSer129 α -synuclein is toxic or simply a response to cellular stress, is still under debate³⁰. pSer129 α -synuclein aggregates have been shown to impair synaptic activity with an activity-dependent inhibition of synaptic vesicle trafficking in vitro, leading to degenerative morphological synaptic changes³³. In human iLBD and PD striatum, we show that

Fig. 7 | α -Synuclein proteoform levels in human putaminal synaptosomes.

A Group and Braak stage difference in total, pSer129, and CTT122 α -synuclein protein levels (over total protein) in putaminal synaptosomes. **B** Group and Braak stage difference in pSer129 and CTT122 fold change over total α -synuclein levels in iLBD and PD compared to control putaminal synaptosomes. Boxplots display the median (central line), the first and third quartiles (box hinges at the 25th and 75th percentiles), and whiskers that extend to minima and maxima. The statistical test used is a two-sided nonparametric rank-based estimation test with age and sex as covariates. Multiple testing comparison corrections were performed with the Tukey test. Exact p values: **A** tot α -syn (up): control vs PD $p = 0.073$, control vs iLBD $p = 0.339$; **A** tot α -syn (down): control vs Braak 1–6 all $p > 0.05$; pSer129 (up): control vs PD $p = 0.043$, control vs iLBD $p = 0.392$; pSer129 (down): control vs Braak 1–5 all $p > 0.05$, control vs Braak 6 $p = 0.033$; CTT122 (up): all $p > 0.05$; CTT122 (down): all $p > 0.05$; **B** pSer129 (up): control vs PD $p = 0.137$, control vs iLBD $p = 0.179$; pSer129

(down): control vs Braak 1–3 $p = 0.817$, control vs Braak 4 $p = 0.095$, control vs Braak 5 $p = 0.090$, control vs Braak 6 $p = 0.035$; CTT122 (up): control vs PD $p = 0.178$, control vs iLBD $p = 0.530$; CTT122 (down): control vs Braak 1–6 all $p > 0.05$. **C, D** Heatmap and scatterplot showing the correlation between pSer129 and CTT122 α -synuclein levels (over total protein) (**C**) and fold change over total α -synuclein levels in synaptosomes per case (labelled as in Supplementary Table 1) (**D**). The statistical test used is a two-sided Spearman's correlation. Exact p values: **C**: $\rho = 0.88$, $p < 0.001$; **D**: $\rho = 0.48$, $p = 0.004$. The grey area around the regression line in **C, D** represents the standard error. The sample consists of $n = 38$ (control = 10, iLBD = 8, PD = 20), and three technical replicates are averaged for each brain donor. Source data are provided as a Source Data file. α -syn α -synuclein, n.a. not available (technical outliers), PTM post-translational modification, tot total. $0.10 < p \leq 0.05^{\#}$, $p < 0.05^*$, $p < 0.01^{**}$, $p < 0.001^{***}$.

synapses positive for pSer129 α -synuclein are also slightly swollen in PD compared with normal synapses in controls, as found before in DLB²³. Additionally, our data show that pSer129 α -synuclein enrichment in dopaminergic synapses negatively correlates with dopaminergic terminal numbers, suggesting that excessive levels of pSer129 α -synuclein might play a role in the PD degenerative process from the earliest pathological stages and could have a neurotoxic component. In line with this, a mechanistic study in a mouse model of synucleinopathy showed that pSer129 was the first α -synuclein PTM to accumulate in the pons one month post-injection of α -synuclein pre-formed fibrils (PFF) in the gastrocnemius muscle³⁴, also indicating that pSer129 α -synuclein might trigger a cascade of events.

Similarly to pSer129, truncation at amino acid position 122 (CTT122) also occurs in the C-terminal domain of α -synuclein. The C-terminal domain of α -synuclein has a major role in maintaining protein solubility, and alterations in this region appear to promote aggregation of α -synuclein into fibrils in vitro^{18,21,30}. CTT122 α -synuclein is enriched in LBs^{20,29}, is detectable at low levels in controls^{19,20}, and is highly increased in post-mortem PD brains and biochemically enriched in buffer-insoluble fractions^{19–21}. Previous reports suggest that CTT might be an early event in PD pathophysiology, as it has been consistently demonstrated that CTT α -synuclein self-assembles into fibrils and promotes α -synuclein aggregation in vitro^{21,35,36}. In line with this, mechanistic studies in mouse models of synucleinopathy suggest that CTTs might be at the top of the aggregation cascade³⁴ or contribute to axonal dystrophy²⁴. However, when looking at DAT and VGLUT1 synapses with confocal microscopy, we show that CTT122 partially mirrored the pattern of pSer129 α -synuclein synaptic enrichment in PD, but in a less accentuated manner and in later disease stages. Moreover, our biochemical analysis of post-mortem human synaptosomes revealed that CTT122 α -synuclein protein levels in putaminal synaptosomes were similar in control, iLBD and PD, arguing against a general synaptic enrichment of this PTM. Our data therefore indicate that CTT122 α -synuclein might not be at the top of the aggregation cascade, as proposed by the experimental cellular and mouse models. However, we also show that when excessively present, CTT122 α -synuclein exerts a strong pathological effect on specific synapses. Glutamatergic synaptic terminals were significantly swollen when enriched in CTT122 α -synuclein in iLBD and PD compared to controls, suggesting that excessive levels of this PTM in specific synapses (i.e. VGLUT1) might have a strong pathological effect on the synaptic environment, which could have been partially replicated in some α -synuclein transgenic mouse models^{24,37}. According to some in vitro^{21,36,38} and post-mortem studies^{20,38}, CTT α -synuclein accumulates specifically at mitochondrial membranes, where it induces mitochondrial dysfunction and oxidative stress^{21,36,38}. CTT122 α -synuclein might therefore aggregate specifically in synaptic mitochondria membranes, as previously shown in neuronal somas of PD brains^{21,36,38}, inducing mitochondrial dysfunction, oxidative stress, and overall synaptic dysfunction, captured by our study as substantial

synaptic swelling. Our observations in PD and iLBD are also supported by findings of others in DLB, where biochemical fractionation revealed an enrichment of aggregated α -synuclein in post-mortem human synaptosomes, and Golgi-Cox-Davenport staining visualised the swelling of such dendrites and spines³⁹. Finally, we also show that CTT122 α -synuclein enrichment in dopaminergic synapses strongly correlated with dopaminergic terminal loss, suggesting that in late PD stages, a possible CTT122-induced mitochondrial dysfunction might additionally play a role in dopaminergic denervation in the striatum, as dopaminergic neurons are known to be particularly sensitive to mitochondrial stress⁴⁰. To conclude, our results suggest that synaptic enrichment of CTT122 α -synuclein accompanies pSer129 enrichment in late PD stages, additionally contributing to glutamatergic synaptic dysfunction and dopaminergic denervation in the striatum.

Antibodies targeting the nonamyloid component (NAC) domain of α -synuclein, such as Syn1¹⁸, also reveal LBs, pale bodies, and astrocytic α -synuclein accumulation^{20,41,42}. Syn1 immunoreactivity is, not surprisingly, abundant in control brain tissue⁴³, prominently in neuropil, consistent with synaptic-like staining profiles^{20,41}. We observed a high density of synapses positive for Syn1 α -synuclein in controls, supporting the notion that α -synuclein is highly present in synapses. However, how total α -synuclein levels change in PD compared to controls is highly inconsistent between studies^{44,45}. Some studies have reported a decrease in Syn1 α -synuclein levels in PD brain tissue⁴⁶ and total α -synuclein levels in CSF^{44,47}. Our microscopy data also show a decreasing pattern of specifically Syn1 α -synuclein-positive dopaminergic synapses in PD. The lower density of dopaminergic synapses positive for Syn1 α -synuclein strongly mirrored dopaminergic synaptic loss, indicating that decreased biomarker levels of α -synuclein in PD might reflect a synaptic, and most specifically, dopaminergic terminal loss, as suggested previously^{45,48}. Our synaptosomal data, however, showed a different pattern, with total α -synuclein protein levels tending to be higher in PD than control putaminal synaptosomes. Altogether, our results suggest that inconsistencies in α -synuclein levels between studies might be due in part to specific (i.e. dopaminergic) synapses being lost (leading to a reduction in α -synuclein levels), in part by remaining synapses accumulating pathological α -synuclein (leading to an increase in α -synuclein levels).

α -Synuclein proteoforms are arranged in an organised manner within LBs²⁰, suggesting a precise timing of accumulation. In our study, pSer129 α -synuclein was found to first be enriched in dopaminergic synapses (at Braak stage 3) prior to dopaminergic terminal denervation, and then in cortical glutamatergic pre-synapses and post-synapses in later disease stages (Braak stage 4–6). Anatomically, dopaminergic synapses connect on the neck of the same dendrites that are innervated by cortical glutamatergic synapses, so that the dopaminergic input coming from the SN can modulate the glutamatergic excitatory input coming from the cortex²⁵. Given the proximity between dopaminergic, cortical glutamatergic, and post-synapses, and the pattern of synaptic α -synuclein enrichment we observed, it is

conceivable to hypothesise about the occurrence of a trans-synaptic neuron-to-neuron spread of putative pathogenic, aggregation-inducing proteoforms of α -synuclein from dopaminergic to glutamatergic synapses. Our evidence generated in this observational study in humans may be consistent with findings in mechanistic mouse models where retrograde transmission of α -synuclein PFF can be observed, and suggests a cell-to-cell propagation of pathology through anatomically connected brain regions^{17,34}. Consistent with mouse models of PD, we show that pSer129 and CTT122 α -synuclein are enriched in cortical glutamatergic pre-synaptic terminals well before the cell bodies located in layer V of the cortex²⁵, which are the first cortical neurons to show LB inclusions¹⁰. Similarly, α -synuclein inclusions in excitatory neurons in the ACC and PFC in layers V–VI were reported after PFF striatal injections in mice⁴⁹. Our results support this evidence in the human brain, and indicate that glutamatergic synapses might pick up pathogenic α -synuclein proteoforms in the putamen, and transport them retrogradely through their axon back to the cell body, where LBs might form in later disease stages.

We confirm loss of DAT synapses in PD, as previously described in ref. 6. Several intrinsic properties, including cell-autonomous features of dopaminergic neurons, have been suggested to contribute to dopaminergic vulnerability and degeneration in PD. In fact, dopaminergic neurons:

- i) Possess long and highly branched axons which are poorly myelinated, and have large synaptic trees⁴⁰;
- ii) have a high metabolic rate and dopamine turnover⁴⁰;
- iii) contain high levels of neuromelanin, a bioproduct of dopamine-quinone production, which makes these neurons more vulnerable to oxidative stress⁵⁰;
- iv) are highly vulnerable to mitochondrial stress⁴⁰;
- v) have a characteristic slow and tonic pacemaker activity, leading to accumulation of Ca^{2+} ⁴⁰, which may contribute to physiological phosphorylation of α -synuclein at Ser129^{31,32};
- vi) have high SNCA expression levels⁴³.

These cell-autonomous features, in combination with increased mitochondrial stress and autophagy-lysosome pathway (ALP) dysfunction, might make dopaminergic neurons (and their synapses) particularly vulnerable to aggregate α -synuclein species. It is therefore plausible to speculate that the combination of (i) intrinsically high endogenous α -synuclein levels, (ii) strong increases in physiological pre-synaptic pSer129 α -synuclein during action potentials, (iii) decreased clearance of α -synuclein due to ALP dysfunction, and (iv) high and/or aberrant metabolic and mitochondrial activity, might make dopaminergic neurons specifically prone to accumulate excessive pSer129 and CTT122 α -synuclein in the pre-synaptic compartment.

Unlike DAT synapses, VGLUT1 synapses with enriched pSer129 and CTT122 α -synuclein did not degenerate in the iLBD and PD putamen. The only study to examine VGLUT1 in human post-mortem striatum reported an increase in VGLUT1 protein expression in the posterior putamen of PD cases⁵¹, although it did not assess the number of VGLUT1 puncta. In line with our results, iPSC-derived cortical glutamatergic neurons from PD patients with LRRK2 variants seem to be more resilient to α -synuclein PFF than iPSC-derived dopaminergic neurons⁵². Interestingly, we showed that VGLUT1 synapses enriched with CTT122 α -synuclein are swollen, which could be indicative of synaptic dysfunction. Animal studies provided evidence for the accumulation of α -synuclein in VGLUT1 synapses, and similarly, VGLUT1 synapses did not degenerate, but their electrophysiological properties were impaired^{53–55}. These findings indicate that VGLUT1 synapses might undergo morphological, electrophysiological, and biochemical alterations when accumulating pathological α -synuclein but do not degenerate, therefore showing to be more resilient to α -synuclein pathology than dopaminergic synapses. Taken together, our results not only point towards the centrality of early

synaptic pathology in PD, but also to a differential vulnerability of different synaptic terminals to α -synuclein pathology.

The main strength of this study lies in the combination of highly sensitive and specific antibodies for multiplex immunofluorescence microscopy and AlphaLISA immunoassays, enabling quantification of α -synuclein proteoform levels in synapses of a pathologically defined cohort that encompasses all Braak α -synuclein stages. A major limitation of our study is the assumption that iLBD represents a neuro-pathological prodrome of PD, whereas it is a matter of debate whether iLBD cases would have developed motor symptoms if they had lived longer⁵⁶. Our results support enrichment of pathological α -synuclein in synapses in both iLBD and PD putamen, which could be seen as evidence of a common pathway of pathological spread of α -synuclein. We also found a 30% dopaminergic neuronal loss in iLBD SN compared to control SN (even if not significant), as previously found^{4,12,56}, which could be indicative of a PD-specific neurodegenerative process. On the other hand, our iLBD cohort was (i) significantly older than our PD cohort, and (ii) mostly composed by females compared to the mostly male PD group, as previously reported for other iLBD cohorts^{9,56}; and (iii) even if iLBD donors in our study presented pSer129 α -synuclein enrichment in dopaminergic synapses, which correlated with dopaminergic loss specifically in iLBD, the dopaminergic loss in the putamen was very limited (~13% not significant, as opposed to previously reported ~30%^{4,11}), overall suggesting that iLBD might represent a resilient group of individuals to α -synuclein pathology. In addition, the putaminal location where we quantified dopaminergic synaptic density might have affected the effect size of dopaminergic denervation of our iLBD cohort: in our study we used putamen anterior to the anterior commissure (in order to image the putamen innervated by the ACC and PFC²⁷), while previous studies have mostly investigated the putamen at the level of, or posterior to the anterior commissure^{4,11}. DAT loss (measured as DAT tracer binding) is more pronounced at the contralateral striatum of the clinically most affected body side⁵⁷. Such asymmetry might have affected our results. Additionally, while our results suggest that the PSD95 pre-processing, which aimed to reduce the cloud-like pattern caused by tyramide precipitation, was thorough in determining the location of post-synaptic densities, we cannot be fully confident that the PSD signal did not at least partially spread into pre-synapses. Lastly, synaptosomal isolation was performed in the contralateral putamen compared to the high-resolution multiplex confocal microscopy, leading to possible differences in the results due to asymmetry.

In conclusion, our results obtained through multiplexed and quantitative immunoassay-based approaches in human pre- and post-synaptic terminals, point towards an enrichment of α -synuclein proteoforms in the early stages of PD, with even greater enrichment in the later stages. We showed that total, pSer129 and CTT122 α -synuclein protein levels are quantifiable in human putaminal synaptosomes of control, iLBD and PD donors. pSer129 α -synuclein is enriched in synapses already from early disease stages, and seems to be enriched in dopaminergic synapses in iLBD before striatal dopaminergic denervation. Our results implicate a possible role of pSer129 α -synuclein in the beginning of the aggregation cascade leading to dopaminergic denervation, and cortical LB pathology. Synaptic enrichment of CTT122 α -synuclein accompanies pSer129 accumulation in late PD stages, worsening glutamatergic synaptic dysfunction and dopaminergic denervation in the striatum.

Methods

Donor inclusion

In collaboration with the Netherlands Brain Bank (NBB, <https://www.brainbank.nl/>) and Normal Ageing Brain Collection Amsterdam (NABCA)⁵⁸ we included a total of 69 brain donors: 32 clinically-defined controls, which were pathologically diagnosed with iLBD (Braak α -synuclein stage 1–6), 27 clinically-defined and pathologically-

confirmed PD brain donors² (Braak α -synuclein stage 4–6), and 10 pathologically confirmed non-diseased controls (Braak α -synuclein stage 0; see Supplementary Table 1 for details). For the PD donors, disease duration (age at death minus age at diagnosis) was extracted from their clinical files. Neuropathological diagnosis was carried out by an expert neuropathologist, and performed according to the international guidelines of the Brain Net Europe II (BNE) consortium (<https://www.brainbank.nl/about-us/brain-net-europe/>). The procedures for brain tissue collection of both NBB (ethical approval #2008/148) and NABCA (ethical approval #2018/150) comply with all relevant ethical regulations, and were approved by the Medical Ethical Committee of the Amsterdam University Medical Centre, Amsterdam. NBB and NABCA operate under strict ethical and legal standards, collecting brain tissue only with written informed consent (or legal authorisation for incapacitated individuals), explicitly permitting autopsy, tissue use for approved scientific research, and anonymised data use, all in compliance with Dutch laws and the General Data Protection Regulation. Ethical approval is ensured through donor consent, independent review by the NBB's scientific committee, confidentiality safeguards, and regulated tissue distribution under a Material Transfer Agreement that prohibits commercial use.

Tissue sampling

The workflow of the methods is visualised in Fig. 6. The putamen was chosen as the main region of interest of this study, as it suffers from severe dopaminergic denervation in PD⁶. Moreover, the anterior region of the putamen receives cortical glutamatergic pre-synaptic input from several cortical regions affected by LB pathology, such as the anterior cingulate (ACC) and prefrontal cortex (PFC)^{27,59}. Brain tissue was collected at autopsy, resulting in an average post-mortem delay (interval between death and autopsy) of 6.5 h (range 3:30–11:45 h:min). Formalin-fixed paraffin-embedded (FFPE) tissue blocks of the putamen (anterior to anterior commissure), and substantia nigra (SN; included: 56/69 cases) were obtained from the right hemisphere and processed for immunohistochemistry. Frozen tissue blocks of the putamen of 38 out of 69 cases were obtained from the left hemisphere and processed for synaptosome isolation (Supplementary Table 1). In addition, ACC and PFC sections already immunostained for α -synuclein by NBB and NABCA biobanks for pathological diagnosis (clone KM51, for details on antibody, see Supplementary Table 2) were included for the cases presenting with Braak α -synuclein stage ≥ 4 (included: ACC 29/37 cases; PFC 33/37 cases).

Immunohistochemistry of striatal tissue sections

During the immunohistochemistry experiments, the order of striatal tissue sections was randomised for each staining protocol to prevent the staining procedures from introducing group-specific biases. Six- μ m-thick sections from FFPE tissue blocks of caudate-putamen were cut and mounted onto superfrost+ glass slides (Thermo Scientific, USA). All sections were immunostained for dopamine transporter (DAT), vesicular glutamate transporter 1 (VGLUT1), and post-synaptic density protein 95 (PSD95). DAT and VGLUT1 markers were chosen because: (i) dopaminergic neurons in the SN project to the putamen⁵⁹, and DAT is localised in their synaptic terminals⁶⁰; (ii) cortical glutamatergic neurons in layer V²⁵ in the ACC and PFC project to the putamen²⁷, and VGLUT1 is localised in their synaptic terminals²⁶. Moreover, each batch was also immunostained with antibodies targeting α -synuclein at aa 91–99 (Syn1, BD Biosciences) as a good approximation of total α -synuclein amounts⁶¹, pSer129 α -synuclein (clone 11A5, Prothena), or CTT122 α -synuclein (clone A15127A, Biologend). For information on primary antibodies, see Supplementary Table 2. Biochemical characterisation and validation of these antibodies targeting α -synuclein proteoforms (clones Syn1, 11A5, A15127A) for immunohistochemistry was previously performed and published^{19,20,29,42,61}. Briefly, FFPE sections were deparaffinised,

immersed in Tris-EDTA pH 9.0, heated to 100 °C in a steam cooker for 30 min, immersed in 80% formic acid for 5 min, and washed under warm running tap water for antigen retrieval. The sections were blocked for endogenous peroxidase using 1% hydrogen peroxide in tris buffered saline (TBS; pH 7.4), and consequently in 3% normal donkey serum in TBS (Triton 0.5%) for 30 min. PSD95 primary antibody was diluted in 1% normal donkey serum in TBS (Triton 0.1%), and sections incubated overnight at 4 °C. On the second day, PSD95 primary antibody was detected using EnVision (Dako, Glostrup, Denmark) and Alexa Fluor[®] 555 Tyramide with 0.005% hydrogen peroxide in Tris-HCl buffer. The sections were then immersed in Tris-EDTA pH 9.0, and heated to 100 °C in a steam cooker for 15 min for antibody removal, and blocked in 3% normal donkey serum in TBS-T (Triton 0.5%) for 30 min. The primary antibodies against DAT, VGLUT1 and one of the above-mentioned α -synuclein primary antibodies (Syn1, pSer129, or CTT122 α -synuclein) were then diluted in 1% normal donkey serum in TBS-T (Triton 0.1%), and incubated overnight at 4 °C. On the third day, sections were incubated for 2 h with the secondary antibodies labelled to Alexa Fluor[®] 680 PLUS, Alexa Fluor[®] 594, and Alexa Fluor[®] 488 PLUS, to detect and visualise DAT, VGLUT1, and one α -synuclein primary antibody, respectively. TBS was used to wash the sections between steps. The sections were counterstained with DAPI and mounted with Mowiol (Sigma-Aldrich, St. Louis, United States) plus anti-fading agent DABCO.

Confocal microscopy of synaptic terminals

Confocal scanning laser microscopy (CSLM) was performed on immunofluorescent stained striatal sections with a Leica TCS SP8 STED 3X microscope (Leica Microsystems, Germany) (Fig. 6A). Confocal imaging of striatal sections was randomized for each imaging protocol, ensuring that the time between staining and imaging did not introduce any group-specific biases. Confocal imaging parameters (Supplementary Table 3) were established for each staining protocol using pilot datasets before the main batch experiment. The exact same imaging parameters were saved and applied uniformly across all images. First, a bright-field overview scan of the striatal tissue section was made using the 10x objective (numerical aperture-NA-0.40) and the “spiral” option in LasX Navigator software (Leica Microsystems, Germany). The overview scanning was stopped at the edges of the putamen (Fig. 6A). Six regions of interest (ROIs) were selected in LasX Navigator using a transparent sheet: four ROIs were placed in the region of the putamen innervated from the ACC, defined as the lower half of the putamen, and two ROIs in the region of the putamen innervated from the PFC, defined as the inner quadrant on top of the ACC innervated region, according to Haber²⁷ (Fig. 6A). The ROIs were scanned sequential with the 60x oil objective lens (NA 1.40) for each fluorochrome with a pulsed white light laser at different wavelengths (Fig. 6A and Supplementary Table 3). Images were taken as z-stacks to allow deconvolution and 3D image analysis (0.6 μ m z-stack, 0.15 μ m z-steps).

Quantitative 3D image analysis in the putamen

After CSLM scanning, images were converted from LIFF to OME.TIF format with Fiji ImageJ Version 1.52p (<https://imagej.net/ij/>). Colour deconvolution was performed with Huygens Professional version 23.04.0p0 64b (<https://svi.nl/Huygens-Professional>), and 3D image analysis in NIS-elements AR analysis 5.42.03 (<https://www.microscope.healthcare.nikon.com/products/software/nis-elements>). Image pre-processing and analysis parameters were set up using pilot datasets and then applied to all images via scripts ($n = 414$ images per condition), ensuring an unbiased analysis. In NIS-elements, images were masked to define the neuropil volume, after which DAT⁺, VGLUT1⁺ and PSD95⁺ synaptic puncta were counted with the ‘bright spots’ function (Fig. 6A and Supplementary Fig. 1), and expressed by number of DAT⁺, VGLUT1⁺ and PSD95⁺ puncta over 100 μ m³ of neuropil. Next, synaptic puncta positive for Syn1, Syn1 clusters, pSer129, and CTT122 α -

synuclein were quantified (for positivity criteria, see Supplementary Table 4). Syn1 α -synuclein staining revealed two types of immunoreactivity (Supplementary Fig. 2): (1) total Syn1 immunoreactivity that was termed “Syn1 α -synuclein”, which resembled the characteristic synaptic-like staining of nonamyloid component (NAC) α -synuclein antibodies in the grey matter, similar to that observed in KM51 staining (for an example see Fig. 1C); and (2) a subset of the total Syn1 immunoreactivity, characterized by spots of high-intensity and high-contrast compared to the background resembling pathological α -synuclein clusters (similar to how LBs appear on KM51 staining, but smaller), referred to us “Syn1 α -synuclein clusters”. For synaptic size analyses, the synaptic perimeter was allowed to grow following the immunoreactivity pattern. Since the PSD95 channel was further pre-processed to reduce the cloud-like pattern due to tyramide precipitation (Supplementary Fig. 3), size analysis was not performed on PSD95⁺ puncta. Additionally, we quantified the density of synaptic pairs, and specifically of DAT or VGLUT1 pre-synapses localised next to a PSD95 post-synapse (Supplementary Fig. 4). To do so, a neighbourhood analysis was performed with the ‘nearest child’ function with a centre-to-centre distance (pre-synapse to post-synapse) of $\leq 1 \mu\text{m}$ (Supplementary Fig. 3). Finally, a quality control step was performed to check if there were masking errors, and when present (masking error rate $< 1\%$), the neuropil masks were adjusted. Imaris 9.9.1 (Oxford Instruments 2023, <https://imaris.oxinst.com/>) was used to make representative 3D surface-rendering images. In summary, the following outcome measures were extracted (Fig. 6A): (1) Density of DAT⁺, VGLUT1⁺ and PSD95⁺ synapses (puncta/100 μm^3); (2) density of DAT⁺, VGLUT1⁺ and PSD95⁺ synapses positive for Syn1, Syn1 clusters, pSer129, and CTT122 α -synuclein (puncta/100 μm^3); (3) mean diameter (μm) of DAT⁺ and VGLUT1⁺ synapses (both positive and negative for α -synuclein proteoforms); (4) percentage of DAT and VGLUT1 in synaptic pairs of all DAT and VGLUT1 synapses; and (5) percentage of DAT and VGLUT1 in synaptic pairs positive for α -synuclein proteoforms of all DAT and VGLUT1 synapses positive for α -synuclein proteoforms.

LB density in anatomically connected regions

Twenty- μm -thick sections from SN FFPE tissue blocks were cut and mounted onto superfrost+ glass slides (Thermo Scientific, USA). Sections were stained for tyrosine hydroxylase (TH) to visualise dopaminergic neurons, and for pSer129 α -synuclein to visualise LBs (clone EP1536Y, Abcam; see Supplementary Table 2). Briefly, the sections were deparaffinised, immersed in Tris-EDTA pH 9.0, and heated to 100 °C in a steam cooker for 30 min for antigen retrieval. The sections were blocked for endogenous peroxidase using 1% hydrogen peroxide in TBS (pH 7.4), and consequently in 3% normal goat serum in TBS (Triton 0.1%) for 30 min. Primary antibodies were diluted in 1% normal donkey serum in TBS (Triton 0.1%), and sections incubated overnight at 4 °C. On the second day, primary antibodies were detected using EnVision (Dako, Glostrup, Denmark) and Vector SG (#SK4700, Vector, Newark, United States) in phosphate-buffered saline (PBS; pH 7.4). TBS and PBS were used to wash the sections between steps. The sections were counterstained with fast nuclear red, dehydrated using a series of ethanol and xylene, and mounted with Entellan (Merck, Darmstadt, Germany).

Using a whole-slide scanner (Olympus VS200 Evident, 20x objective), images of immunostained SN (TH and pSer129 α -synuclein), ACC and PFC sections (KM51 α -synuclein) were digitised and quantified using QuPath 0.2.3 stardist⁶². In the SN sections (Fig. 6B), a ROI was drawn along the edges of the cerebral peduncle until the white matter tracts below the red nucleus using the colour contrast optical density sum to delineate the SN, as done before⁶³. Using *in-house* QuPath scripts, outcome measures of TH neuronal density (count/mm²) and LB density (count/mm²) were extracted as previously described in ref. 63. In ACC and PFC sections (Fig. 6C), ROIs containing

all cortical layers were delineated in straight areas of the cortex to avoid over- or underestimation of pathology in sulci and gyri, as described before in refs. 64,65. DAB immunoreactivity was quantified with *in-house* QuPath scripts, using an object classifier, as done previously in refs. 64,65, extracting LB density (count/mm²).

Synaptosome isolation and characterisation

Synaptosome isolation. Synaptosomes were isolated from human frozen putamen tissue for a subset of cases (PD $n=20$, iLBD $n=8$, control $n=10$, total $n=38$, see Supplementary Table 1 for details) according to a previously described method (Fig. 6D)^{28,66}. Frozen sample order was randomised to prevent introducing group-specific biases. Briefly (Fig. 6D), 100 mg of frozen putamen was included for each case. Frozen putamen was cut in thick slices (80–100 μm) with a cryostat, while carefully avoiding white matter, caudate and nucleus accumbens if present in the tissue blocks. The brain tissue was first washed once in 0.5 mL of ice-cold homogenization buffer (HB; 0.32 M sucrose, 4 mM HEPES, 20 mM DTT, 50 mM EDTA, protease inhibitor cocktail-Roche, Branchburg, NJ-, phosphatase inhibitor cocktail cOmplete™, Mini, EDTA-free Protease Inhibitor Cocktail, Roche, Branchburg, NJ-, pH 7.4) to reduce blood contamination, and centrifuged at 1000 $\times g$ (3068 RPM) for 5 min at 4 °C in a Benchtop Centrifuge 5804R (Eppendorf, the Netherlands). The HB was discarded, and 0.5 mL of new ice-cold HB was added to the pellet for the homogenization step. Brain tissue was homogenised with ten slow and uniform strokes with a Teflon pestle after transferring the tissue to a 2 mL Eppendorf tube, and then an additional 0.5 mL of HB was added to the tube. Both the tubes and pestle were pre-chilled in a beaker of ice before homogenization. The resulting homogenate was then centrifuged for 5 min at 1000 $\times g$, and the pellet (P1) discarded. The supernatant (S1, total homogenate fraction) was partially collected for western blot analysis (20 μL), and the rest was further centrifuged at 14,500 $\times g$ for 12 min. After this, 25 μL of supernatant (S2, cytosolic fraction) was collected for western blot analysis, and the pellet (P2) was re-suspended in 250 μL of ice-cold HB by pipetting up and down. The re-suspended P2 was carefully loaded on top of a three-step (3%, 10%, and 23%) Percoll gradient (Sigma Aldrich, Natick, MA) (Fig. 6D). The 12-mL polypropylene tubes containing the Percoll gradient with the re-suspended P2 were inserted into rubber inserts in a Eppendorf F-34-6-38 fixed angle rotor (34°, 11.5 cm radius, Eppendorf, the Netherlands), and centrifuged for 15 min at 15,557 $\times g$ with slow acceleration and deceleration (both set at 1) to avoid disturbing the layers. After centrifugation, the synaptosome-rich interface between 10% and 23% Percoll (F3-4²⁸; Supplementary Fig. 5) was carefully collected with a pipette. To remove the Percoll from the isolated fraction, the sample was washed in a 12-mL volume of sucrose/EDTA buffer (0.32 M Sucrose, 1 mM EDTA, 5 mM Tris, pH 7.4) and centrifuged at 15,557 $\times g$ for 15 min with slow acceleration and deceleration (both set at 1) to avoid disturbing the pellet. The supernatant was discarded, and the synaptosomal pellet was collected. A Pierce BCA assay kit (Thermo Fisher Scientific, #23225) was used to determine the total protein content of each sample.

Immunohistochemistry. To confirm the presence of pre- and post-synaptic markers in the synaptosomal preparation, we performed immunofluorescent staining with anti-synaptophysin and anti-PSD95 antibodies, and confocal microscopy evaluation (Fig. 6D). Similar as described before in ref. 66, a 4 μL volume of synaptosomal pellet was allowed to bind to poly-L-lysine-coated μSlide 8 Well chamber slide (#80826, Ibidi, Gräfelfing, Germany) overnight at 4 °C. The samples were fixed with 4% paraformaldehyde for 15 min, washed twice with PBS, permeabilised in PBS with 0.3% Triton X-100 for 10 min, and blocked for 1 h in PBS with 0.1% Triton X-100 and 5% normal donkey serum. Synaptosomes were incubated with primary antibodies mouse anti-synaptophysin (#M7315, Agilent) and rabbit anti-PSD95 (#3450S,

Cell Signalling Technology) in PBS with 0.1% Triton X-100 and 1% normal donkey serum overnight at 4 °C (Supplementary Table 5). The day after, the synaptosomes were washed twice, and then labelled with anti-mouse Alexa Fluor-488 (#A21202, ThermoFisher) and anti-rabbit Alexa Fluor-594 PLUS (#A32754, ThermoFisher) secondary antibodies, respectively, for 1 h at room temperature (RT). After 2 washes, the synaptosomes were visualised with 3D CSLM in a Leica TCS SP8 microscope (Leica Microsystems, Germany) using a HC PL PAO CS2 60 × oil objective lens (NA 1.40). All signals were detected using gated hybrid detectors in counting mode. z-stacks ($z = 0.6 \mu\text{m}$; 1200×1200 pixels) were imaged for one representative control, one iLBD and two PD cases (case numbers 5, 25, 51, and 65 in Supplementary Table 1, respectively). After scanning, the images were deconvoluted using CMLE algorithms in Huygens Professional⁶⁷, and their maximum projections (ImageJ Fiji, National Institute of Health, USA⁶⁸) were used to visualise the synaptosomes (Fig. 6D).

Western blot. Western blot analyses were performed on a subset of synaptosomal fractions to confirm the enrichment of pre- and post-synaptic proteins compared to total homogenate (S1) and cytosolic fractions (S2). Specifically, 20 μg of total protein of the S1 and S2 fractions, and 1 μg of total protein of the synaptosomal fraction (due to limited sample) were mixed with NuPAGE LDS sample buffer (Invitrogen; NP0007) and NuPAGE Sample Reducing Agent (Invitrogen; NP0004), heated for 10 min at 70 °C, and loaded on a NUPAGE pre-cast 4–12% gradient Bis-Tris gel (Invitrogen; NP0336) at 200 Volts for 35 min. Separated proteins were subsequently blotted (at 30 Volts for 90 min) onto 0.22 μm nitrocellulose membranes (LI-COR; #926-31092) using 1x NuPAGE Transfer Buffer (Invitrogen; #NP0006) containing 10% (v/v) methanol and 0.1% (v/v) antioxidant (Invitrogen; #NP0005). The blot was rinsed with ultrapure water and incubated for 5 min in Revert700 Total Protein stain solution (LI-COR; #926-11011). After washing with Revert Washing Solution (LI-COR; #926-11012) and ultrapure water, acquisition of the total protein staining was done with Odyssey SA (LI-COR Biotechnology, Germany) and ImageStudio software (LI-COR; version 5.2.5). After de-staining with Revert700 Destaining Solution (LI-COR; #926-11013) and rinsing in ultrapure water, the blot was blocked in Intercept (TBS) Blocking Buffer (LI-COR; #927-60001) for 1 h at RT. Blots were then incubated overnight at 4 °C with a mix of primary antibodies, mouse anti-synaptophysin (DAKO/Agilent; 1:500) and rabbit anti-PSD95 (Cell Sign.; 1:1500) (Supplementary Table 2) diluted in Intercept (TBS) Blocking Buffer/TBS-T (50/50). After washing in TBS-T, the blot was incubated with a mix of secondary antibodies, donkey anti-mouse/IR800cw (LI-COR; 1:10,000) and donkey anti-rabbit/IR680lt (LI-COR; 1:10,000). Finally, after a last wash in TBS-T, acquisition of the immunostaining was done with Odyssey SA and ImageStudio software. Specific band intensities (for synaptophysin, the ± 38 kDa band; for PSD95, the ± 90 kDa band) were quantified and normalised (-corrected for slight input differences) using the total protein stain.

Quantification of α -synuclein levels in synaptosomes

α -Synuclein protein levels were quantified in the synaptosome fraction using AlphaLISA immunoassays (Revvity)⁶⁹ following the protocol established by Moors et al.¹⁹, with modifications as per the manufacturer's instructions (Fig. 6E). The assay was developed to detect pSer129, CTT122, and a C-terminal epitope of α -synuclein between residues 118–123 (clone MJFR1, designated as “total” α -synuclein). For this purpose, a biotinylated antibody targeting the NAC region of α -synuclein (Biotin anti- α -synuclein, Clone A15115A, BioLegend, Cat. 848306; epitope aa 80–96) was used as a common Detection Antibody across all assays. For the specific detection of the α -synuclein proteoforms, the following Acceptor Antibodies were employed: Syn-142 (for pSer129, Roche¹⁹), MJFR1 (for “total” C-Term, Abcam, Cat. ab209420), and A15127A (for CTT122, BioLegend, Cat. 848402)

(Supplementary Table 6). These antibodies were coupled to AlphaLISA Acceptor Beads (Unconjugated AlphaLISA Acceptor Beads, Revvity, Cat. 6772002) at a 10:1 beads-to-antibody weight ratio according to the manufacturer's guidelines. MJFR1 acceptor antibody demonstrated to recognize 76% of pSer129 and 0% of CTT122 α -synuclein in this assay (Supplementary Fig. 6). For all the antibody pairs, optimal concentration of the antibodies and antibody-bead conjugate was determined to maximize signal/noise ratio and to lay below the hook point (point of where an excess of target molecules oversaturates the Donor and the Acceptor beads, inhibiting their association and causing a progressive signal decrease). Assays were conducted in 384-well plates (AlphaPlate 384-well, Revvity, Cat. 6005350) with a total volume of 50 μL per well. Prior to the assay, samples were diluted in Assay Buffer composed of 25 mM HEPES (Sigma-Aldrich, Cat. H3375), 0.5% (v/v) Triton X-100 (Merck Millipore, Cat. 8603), 0.1% (w/v) Casein (Sigma-Aldrich, Cat. C0376), and 0.1% (w/v) Dextran (Dextran-500, Carl Roth, Cat. 9219.3). Standard curves for “total” α -synuclein (rPeptide, Cat. S-1001-2), pSer129 (Proteos, Cat. RP-004), and CTT122 (Roche¹⁹) were prepared using purified recombinant proteins in Assay Buffer with the same sucrose/EDTA buffer dilution as used for the synaptosome samples. Optimal dilutions were determined for each assay: 1:250 for total, 1:2 for pSer129, and 1:10 for CTT122 α -synuclein. For each assay, 5 μL of diluted samples or recombinant standards were added to wells, followed by 10 μL of a solution containing Acceptor Beads coupled with Acceptor Antibodies (75 $\mu\text{g}/\text{mL}$ for total and CTT122 assays, 50 $\mu\text{g}/\text{mL}$ for pSer129). The plate was shaken for 1 min and incubated for 2 h at RT in the dark. Subsequently, 10 μL of Detection Antibody solution (0.75 $\mu\text{g}/\text{mL}$ biotinylated antibody in Assay Buffer) was added, and the plate was shaken for 1 min and incubated for an additional 1 h at RT in the dark. Finally, 25 μL of an 80 $\mu\text{g}/\text{mL}$ Streptavidin-labelled Donor Beads solution (AlphaScreen Streptavidin Donor Beads, Revvity, Cat. 6760002) was added to each well, followed by 1 min of mixing and a 30-min incubation at RT in the dark. All measurements were performed in technical triplicate and acquired using a VICTOR Nivo reader (PerkinElmer). Quantification of protein levels was based on the standard curves fitted using a 4-parameter logistic model. The lower limit of detection (LLOD) and lower limit of quantification (LLOQ) were calculated as $\text{LLOD} = \frac{3.3\sigma}{\delta}$ and $\text{LLOQ} = \frac{10\sigma}{\delta}$, where σ is the standard deviation and δ is the slope of the calibration curve (Supplementary Fig. 6). Raw values (signal a.u.) of triplets with a high coefficient of variation ($\text{CV}\% > 30\%$) were quality-checked, and outlying values were excluded (3 values in pSer129 plate). Final average CVs were 2.7% (range 0.5–8.8%) for total, 10.4% for pSer129 (1.1–24.6%), and 4.8% (0.1–12.5%) for CTT122 α -synuclein.

Statistical analysis

Immunohistochemistry. Brain donors were selected to include approximately ten samples per Braak α -synuclein stage; this target was met for all stages except Braak stage 2, for which only three donors were available. To prevent technical bias, striatal tissue sections and confocal imaging were randomised for each staining protocol, with standardised imaging parameters established from pilot datasets and uniformly applied across all samples. Image pre-processing and analysis were similarly standardised using scripted workflows. Statistical analysis was performed in R Studio 4.2.1 (<https://www.r-studio.com/>). The data were log transformed after the addition of a constant (+1) to avoid undefined numbers when log transforming zeros. Outliers with ± 3 standard deviations (SD) were excluded. With a nested dataset (6 ROIs per case), DAT, VGLUT1 and PSD95 synaptic density differences between groups were assessed with linear mixed models (LMM) with age and sex as covariates, and nested for dataset (Syn1/pSer129/CTT122 α -synuclein) and case ID. Synaptic density differences between Braak α -synuclein stages were assessed with LMM, with Braak α -synuclein stage as factor, age and sex as covariates, and nested for dataset (Syn1/pSer129/CTT122 α -synuclein) and case ID. Differences in

Braak α -synuclein stages were assessed compared to controls (Braak α -synuclein stage 1 vs control, Braak α -synuclein stage 2 vs control, and so on). Similar analyses were performed to assess group and Braak α -synuclein stage difference in α -synuclein proteoform⁺ synaptic densities (except for not including “dataset” as a nested variable since analyses were performed in individual datasets). To investigate the correlations between α -synuclein proteoform⁺ synaptic density and synaptic density or LB density, these values were averaged to have one value per case, and Spearman’s correlations were performed with age and sex as covariates. To assess the difference between α -synuclein proteoform⁺ VGLUT1 synaptic density in ACC and PFC putaminal innervation area, and LB density in ACC and PFC (respectively) in Braak stages 3 and 4, the original log-transformed values were scaled as percentage (0–100%), and then differences within Braak stage 3 and 4 were tested with LMM with age and sex as covariates, and case ID as nested variable. For synaptic size analyses, LMM were used to assess differences in synaptic diameter between synapses (only DAT and VGLUT1) positive and negative for α -synuclein proteoforms, and in synaptic diameter of positive synapses to α -synuclein proteoforms between groups, with age and sex as covariates, and nested for case ID. For analyses on synaptic pairs, LMM were used to assess the differences in the percentage of α -synuclein proteoform⁺ synapses that were within a synaptic pair (i.e. next to a PSD95 puncta) or not, with age, sex, and percentage of synaptic pairs as covariates, and case ID as a nested variable. Multiple pairwise (post-hoc) and multiple testing comparison corrections were performed with the Tukey test, after which p values < 0.05 were considered significant.

α -Synuclein levels in synaptosomes. Samples were selected based on the availability of frozen putamen from donors already included in the immunohistochemistry and confocal imaging analyses. To prevent technical bias, synaptosomal samples were randomised during isolation and α -synuclein protein quantification. The data were log transformed after the addition of a constant (+1) to avoid undefined numbers when log transforming zeros. Nonparametric rank-based estimation tests with age and sex as covariates were used to assess group and Braak stages differences. Multiple pairwise (post-hoc) corrections were performed with the Tukey test, after which p values < 0.05 were considered significant. Spearman’s correlation was performed to assess the correlation between synaptosomal α -synuclein proteoform levels. One control (case number 9 in Supplementary Table 1) and two PD cases (case nr 47 and 52 in Supplementary Table 1) were found to be statistical outliers (i.e. >3 SD from the mean) in synaptosomal normalised pSer129 α -synuclein levels. These cases had outlying low total protein levels (0.76, 0.64, and 0.94 mg/mL, respectively, with average across cases 3.68 mg/mL) while having mid-to-high synaptosomal pSer129 α -synuclein levels (105 pg/mL, 163 pg/mL, and 542 pg/mL, respectively, with average across cases 110 pg/mL), and were therefore excluded.

Reporting summary

Further information on research design is available in the Nature Portfolio Reporting Summary linked to this article.

Data availability

All processed data in the figures presented in this study are included in the accompanying Source Data file. Access to the raw data is subject to restrictions to protect the identities of brain donors from the NBB and NABCA, and is available exclusively for research purposes. This material and data should only be used for research purposes, only in the Recipient’s organization, cannot be transferred to anyone else within or outside the Recipient organization without the prior written consent of the Provider, and should be used in compliance with all applicable statutes and regulations in Recipient’s place and country. Requests for raw data or raw IHC images should be directed to Dr.

Wilma van de Berg (wdj.vandenberg@amsterdamumc.nl). Source data are provided with this paper.

Code availability

The scripts used in this study are openly available at the GitHub repository: <https://github.com/WilmaVandenberg/Synaptic-alpha-synuclein/>.

References

- Bloem, B. R., Okun, M. S. & Klein, C. Parkinson’s disease. *Lancet* **397**, 2284–2303 (2021).
- Postuma, R. B. et al. MDS clinical diagnostic criteria for Parkinson’s disease. *Mov. Disord.* **30**, 1591–1601 (2015).
- Poewe, W. et al. Parkinson disease. *Nat. Rev. Dis. Prim.* **3**, 1–21 (2017).
- Dickson, D. W. et al. Evidence that incidental Lewy body disease is pre-symptomatic Parkinson’s disease. *Acta Neuropathol.* **115**, 437–444 (2008).
- Parkkinen, L. et al. Disentangling the relationship between Lewy bodies and nigral neuronal loss in Parkinson’s disease. *J. Parkinson’s Dis.* **1**, 277–286 (2011).
- Kraemmer, J. et al. Correlation of striatal dopamine transporter imaging with post mortem substantia nigra cell counts. *Mov. Disord.* **29**, 1767–1773 (2014).
- Scherman, D. et al. Striatal dopamine deficiency in Parkinson’s disease: role of aging. *Ann. Neurol.* **26**, 551–557 (1989).
- Bellucci, A., Antonini, A., Pizzi, M. & Spano, P. The end is the beginning: Parkinson’s disease in the light of brain imaging. *Front. Aging Neurosci.* **9**, 330 (2017).
- Frigerio, R. et al. Incidental Lewy body disease: Do some cases represent a preclinical stage of dementia with Lewy bodies?. *Neurobiol. Aging* **32**, 857–863 (2011).
- Braak, H. et al. Staging of brain pathology related to sporadic Parkinson’s disease. *Neurobiol. Aging* **24**, 197–211 (2003).
- DelleDonne, A. et al. Incidental Lewy body disease and preclinical Parkinson disease. *Arch. Neurol.* **65**, 1074–1080 (2008).
- Dijkstra, A. A. et al. Stage-dependent nigral neuronal loss in incidental Lewy body and Parkinson’s disease. *Mov. Disord.* **29**, 1244–1251 (2014).
- Longhena, F., Faustini, G., Spillantini, M. G. & Bellucci, A. Living in promiscuity: the multiple partners of alpha-synuclein at the synapse in physiology and pathology. *Int. J. Mol. Sci.* **20**, 141 (2019).
- Garcia-Reitböck, P. et al. SNARE protein redistribution and synaptic failure in a transgenic mouse model of Parkinson’s disease. *Brain* **133**, 2032–2044 (2010).
- Rockenstein, E. et al. Accumulation of oligomer-prone α -synuclein exacerbates synaptic and neuronal degeneration in vivo. *Brain* **137**, 1496–1513 (2014).
- Wu, Q. et al. Neuronal activity modulates alpha-synuclein aggregation and spreading in organotypic brain slice cultures and in vivo. *Acta Neuropathol.* **140**, 831–849 (2020).
- Kim, S. et al. Transneuronal propagation of pathologic alpha-synuclein from the gut to the brain models Parkinson’s disease. *Neuron* **103**, 627–641 e627 (2019).
- Barrett, P. J. & Greenamyre, J. T. Post-translational modification of α -synuclein in Parkinson’s disease. *Brain Res.* **1628**, 247–253 (2015).
- Moors, T. E. et al. Multi-platform quantitation of alpha-synuclein human brain proteoforms suggests disease-specific biochemical profiles of synucleinopathies. *Acta Neuropathol. Commun.* **10**, 82 (2022).
- Moors, T. E. et al. The subcellular arrangement of alpha-synuclein proteoforms in the Parkinson’s disease brain as revealed by multi-color STED microscopy. *Acta Neuropathol.* **142**, 423–448 (2021).
- Sorrentino, Z. A. & Giasson, B. I. The emerging role of α -synuclein truncation in aggregation and disease. *J. Biol. Chem.* **295**, 10224–10244 (2020).

22. Muntane, G., Dalfo, E., Martinez, A. & Ferrer, I. Phosphorylation of tau and α -synuclein in synaptic-enriched fractions of the frontal cortex in Alzheimer's disease, and in Parkinson's disease and related α -synucleinopathies. *Neuroscience* **152**, 913–923 (2008).
23. Colom-Cadena, M. et al. Synaptic phosphorylated α -synuclein in dementia with Lewy bodies. *Brain* **140**, 3204–3214 (2017).
24. Games, D. et al. Axonopathy in an α -synuclein transgenic model of Lewy body disease is associated with extensive accumulation of C-terminal-truncated α -synuclein. *Am. J. Pathol.* **182**, 940–953 (2013).
25. Moss, J. & Bolam, J. P. A dopaminergic axon lattice in the striatum and its relationship with cortical and thalamic terminals. *J. Neurosci.* **28**, 11221–11230 (2008).
26. Fremeau, R. T. Jr. et al. Vesicular glutamate transporters 1 and 2 target to functionally distinct synaptic release sites. *Science* **304**, 1815–1819 (2004).
27. Haber, S. N. Corticostriatal circuitry. *Dialogues Clin. Neurosci.* **18**, 7–21 (2016).
28. Dunkley, P. R., Jarvie, P. E. & Robinson, P. J. A rapid percoll gradient procedure for preparation of synaptosomes. *Nat. Protoc.* **3**, 1718–1728 (2008).
29. Anderson, J. P. et al. Phosphorylation of Ser-129 is the dominant pathological modification of alpha-synuclein in familial and sporadic Lewy body disease. *J. Biol. Chem.* **281**, 29739–29752 (2006).
30. Oueslati, A. Implication of alpha-synuclein phosphorylation at S129 in synucleinopathies: What have we learned in the last decade?. *J. Parkinsons Dis.* **6**, 39–51 (2016).
31. Parra-Rivas, L. A. et al. Serine-129 phosphorylation of alpha-synuclein is an activity-dependent trigger for physiologic protein-protein interactions and synaptic function. *Neuron* **111**, 4006–4023 e4010 (2023).
32. Ramalingam, N. et al. Dynamic physiological alpha-synuclein S129 phosphorylation is driven by neuronal activity. *NPJ Parkinsons Dis.* **9**, 4 (2023).
33. Wallace, J. N. et al. Excess phosphoserine-129 alpha-synuclein induces synaptic vesicle trafficking and declustering defects at a vertebrate synapse. *Mol. Biol. Cell* **35**, ar10 (2024).
34. Lloyd, G. M. et al. Carboxyl truncation of alpha-synuclein occurs early and is influenced by human APOE genotype in transgenic mouse models of alpha-synuclein pathogenesis. *Acta Neuropathol. Commun.* **11**, 119 (2023).
35. Liu, C. W. et al. A precipitating role for truncated alpha-synuclein and the proteasome in alpha-synuclein aggregation: implications for pathogenesis of Parkinson disease. *J. Biol. Chem.* **280**, 22670–22678 (2005).
36. Zhang, C. et al. C-terminal truncation modulates alpha-synuclein's cytotoxicity and aggregation by promoting the interactions with membrane and chaperone. *Commun. Biol.* **5**, 798 (2022).
37. Spencer, B. et al. Anti-alpha-synuclein immunotherapy reduces alpha-synuclein propagation in the axon and degeneration in a combined viral vector and transgenic model of synucleinopathy. *Acta Neuropathol. Commun.* **5**, 7 (2017).
38. Devi, L., Raghavendran, V., Prabhu, B. M., Avadhani, N. G. & Anandatheerthavarada, H. K. Mitochondrial import and accumulation of alpha-synuclein impair complex I in human dopaminergic neuronal cultures and Parkinson disease brain. *J. Biol. Chem.* **283**, 9089–9100 (2008).
39. Kramer, M. L. & Schulz-Schaeffer, W. J. Presynaptic α -synuclein aggregates, not Lewy bodies, cause neurodegeneration in dementia with Lewy bodies. *J. Neurosci.* **27**, 1405–1410 (2007).
40. Surmeier, D. J., Obeso, J. A. & Halliday, G. M. Selective neuronal vulnerability in Parkinson disease. *Nat. Rev. Neurosci.* **18**, 101–113 (2017).
41. Kovacs, G. G. et al. An antibody with high reactivity for disease-associated α -synuclein reveals extensive brain pathology. *Acta Neuropathol.* **124**, 37–50 (2012).
42. Altay, M. F., Liu, A. K. L., Holton, J. L., Parkkinen, L. & Lashuel, H. A. Prominent astrocytic alpha-synuclein pathology with unique post-translational modification signatures unveiled across Lewy body disorders. *Acta Neuropathol. Commun.* **10**, 163 (2022).
43. Taguchi, K., Watanabe, Y., Tsujimura, A. & Tanaka, M. Brain region-dependent differential expression of alpha-synuclein. *J. Comp. Neurol.* **524**, 1236–1258 (2016).
44. Mollenhauer, B. et al. Longitudinal analyses of cerebrospinal fluid alpha-synuclein in prodromal and early Parkinson's disease. *Mov. Disord.* **34**, 1354–1364 (2019).
45. Camporesi, E. et al. Fluid biomarkers for synaptic dysfunction and loss. *Biomark. Insights* **15**, 1177271920950319 (2020).
46. Zhou, J. et al. Changes in the solubility and phosphorylation of alpha-synuclein over the course of Parkinson's disease. *Acta Neuropathol.* **121**, 695–704 (2011).
47. Eusebi, P. et al. Diagnostic utility of cerebrospinal fluid alpha-synuclein in Parkinson's disease: a systematic review and meta-analysis. *Mov. Disord.* **32**, 1389–1400 (2017).
48. Ohrfelt, A. et al. Cerebrospinal fluid alpha-synuclein in neurodegenerative disorders—A marker of synapse loss?. *Neurosci. Lett.* **450**, 332–335 (2009).
49. Stoyka, L. E. et al. Behavioral defects associated with amygdala and cortical dysfunction in mice with seeded alpha-synuclein inclusions. *Neurobiol. Dis.* **134**, 104708 (2020).
50. Zecca, L., Zucca, F. A., Albertini, A., Rizzio, E. & Fariello, R. G. A proposed dual role of neuromelanin in the pathogenesis of Parkinson's disease. *Neurology* **67**, S8–S11 (2006).
51. Kashani, A., Betancur, C., Giros, B., Hirsch, E. & El Mestikawy, S. Altered expression of vesicular glutamate transporters VGLUT1 and VGLUT2 in Parkinson disease. *Neurobiol. Aging* **28**, 568–578 (2007).
52. A. Abey in *AD/PD™ 2024 Alzheimer's & Parkinson's Diseases Conference*.
53. Tozzi, A. et al. Dopamine-dependent early synaptic and motor dysfunctions induced by alpha-synuclein in the nigrostriatal circuit. *Brain* **144**, 3477–3491 (2021).
54. Chen, L. et al. Synaptic location is a determinant of the detrimental effects of alpha-synuclein pathology to glutamatergic transmission in the basolateral amygdala. *Elife*. <https://doi.org/10.7554/eLife.78055> (2022).
55. Durante, V. et al. Alpha-synuclein targets GluN2A NMDA receptor subunit causing striatal synaptic dysfunction and visuospatial memory alteration. *Brain* **142**, 1365–1385 (2019).
56. Iacono, D. et al. Parkinson disease and incidental Lewy body disease: Just a question of time?. *Neurology* **85**, 1670–1679 (2015).
57. Wallert, E. D. et al. Imaging dopaminergic neurotransmission in neurodegenerative disorders. *J. Nucl. Med.* **63**, 27S–32S (2022).
58. Jonkman, L. E. et al. Normal Aging Brain Collection Amsterdam (NABCA): a comprehensive collection of postmortem high-field imaging, neuropathological and morphometric datasets of non-neurological controls. *NeuroImage Clin.* **22**, 101698 (2019).
59. Haber, S. N. The place of dopamine in the cortico-basal ganglia circuit. *Neuroscience* **282**, 248–257 (2014).
60. Giros, B. & Caron, M. G. Molecular characterization of the dopamine transporter. *Trends Pharm. Sci.* **14**, 43–49 (1993).
61. Altay, M. F. et al. Development and validation of an expanded antibody toolset that captures alpha-synuclein pathological diversity in Lewy body diseases. *NPJ Parkinsons Dis.* **9**, 161 (2023).
62. Bankhead, P. et al. QuPath: open source software for digital pathology image analysis. *Sci. Rep.* **7**, 16878 (2017).
63. Lin, C. P. et al. Nigral pathology contributes to microstructural integrity of striatal and frontal tracts in Parkinson's disease. *Mov. Disord.* **38**, 1655–1667 (2022).
64. Frigerio, I. et al. Neurofilament light chain is increased in the parahippocampal cortex and associates with pathological hallmarks in

- Parkinson's disease dementia. *Transl. Neurodegeneration* **12**, 3 (2023).
65. Frigerio, I. et al. Regional differences in synaptic degeneration are linked to alpha-synuclein burden and axonal damage in Parkinson's disease and dementia with Lewy bodies. *Acta Neuropathol. Commun.* **12**, 4 (2024).
 66. Fonseca-Ornelas, L. et al. Altered conformation of α -synuclein drives dysfunction of synaptic vesicles in a synaptosomal model of Parkinson's disease. *Cell Rep.* **36**, 109333 (2021).
 67. Scientific Volume Imaging. *Huygens Professional*. <https://svi.nl/Huygens-Professional>
 68. Schindelin, J. et al. Fiji: an open-source platform for biological-image analysis. *Nat. Methods* **9**, 676–682 (2012).
 69. Bielefeld-Sevigny, M. AlphaLISA immunoassay platform—the “no-wash” high-throughput alternative to ELISA. *Assay. Drug Dev. Technol.* **7**, 90–92 (2009).
 70. Montine, T. J. et al. National Institute on Aging–Alzheimer's Association guidelines for the neuropathologic assessment of Alzheimer's disease: a practical approach. *Acta Neuropathol.* **123**, 1–11 (2012).

Acknowledgements

This study was funded by The Michael J. Fox Foundation (grant #17253; #022468). We would like to thank Chen-Pei Lin for the contribution of previously stained substantia nigra section and training in substantia nigra segmentation; Annemieke Rozemuller for the pathological characterization of the cohort; Evelien Timmermans, Angela Ingrassia, and Marko Popovic for their technical support. We thank Wagner Zago at Prothena Biosciences Inc. for providing the 11A5 antibody. We would also like to thank the autopsy teams of the Netherlands brainbank (NBB) and Normal Aging Brain Collection Amsterdam (NABCA). Finally, we would like to thank all brain donors and their next of kin for brain donation.

Author contributions

I.F. contributed to experimental concept and design, the selection and definition of the cohort, data collection, statistical analysis, interpretation of the data, and drafting of the manuscript. M.L.M. contributed to the selection and definition of the cohort, and to α -synuclein quantification in synaptosomes. A.B.W. and D.T.V. contributed to the acquisition of confocal microscopy images. J.J.P.B. contributed to the isolation of synaptosomes, and α -synuclein quantification in synaptosomes. W.A.B. and B.L.G. contributed to the experimental concept and optimisation of α -synuclein quantification in synaptosomes. I.L.C. supported the statistical analysis. A.J.J. contributed to immunohistochemistry data collection. H.W.B. contributed to the interpretation of the data. M.B. and D.M. contributed to the interpretation of the data and provided some of the antibodies and recombinant proteins. L.E.J. contributed to the inter-

pretation of the data and obtained the funding. W.D.J.B. contributed to the experimental concept and design, cohort selection, pathological characterisation, interpretation of the data, drafting of the manuscript and obtained the funding. All authors read and approved the final manuscript.

Competing interests

The authors I.F., M.L.M., A.B.W., D.T.V., J.J.P.B., W.A.B., B.L.G., I.L.C., A.J.J., H.W.B., L.E.J., and W.D.J.B. declare that they have no competing interests. D.M. and M.B. are full-time employees of Roche/F. Hoffmann-La Roche Ltd, and they may additionally hold Roche stock/stock options.

Additional information

Supplementary information The online version contains supplementary material available at <https://doi.org/10.1038/s41467-025-61052-1>.

Correspondence and requests for materials should be addressed to Irene Frigerio.

Peer review information *Nature Communications* thanks Tara Spire Jones and the other, anonymous, reviewer for their contribution to the peer review of this work. A peer review file is available.

Reprints and permissions information is available at <http://www.nature.com/reprints>

Publisher's note Springer Nature remains neutral with regard to jurisdictional claims in published maps and institutional affiliations.

Open Access This article is licensed under a Creative Commons Attribution-NonCommercial-NoDerivatives 4.0 International License, which permits any non-commercial use, sharing, distribution and reproduction in any medium or format, as long as you give appropriate credit to the original author(s) and the source, provide a link to the Creative Commons licence, and indicate if you modified the licensed material. You do not have permission under this licence to share adapted material derived from this article or parts of it. The images or other third party material in this article are included in the article's Creative Commons licence, unless indicated otherwise in a credit line to the material. If material is not included in the article's Creative Commons licence and your intended use is not permitted by statutory regulation or exceeds the permitted use, you will need to obtain permission directly from the copyright holder. To view a copy of this licence, visit <http://creativecommons.org/licenses/by-nc-nd/4.0/>.

© The Author(s) 2025